Abstracta

Ano XXVI - N. 01

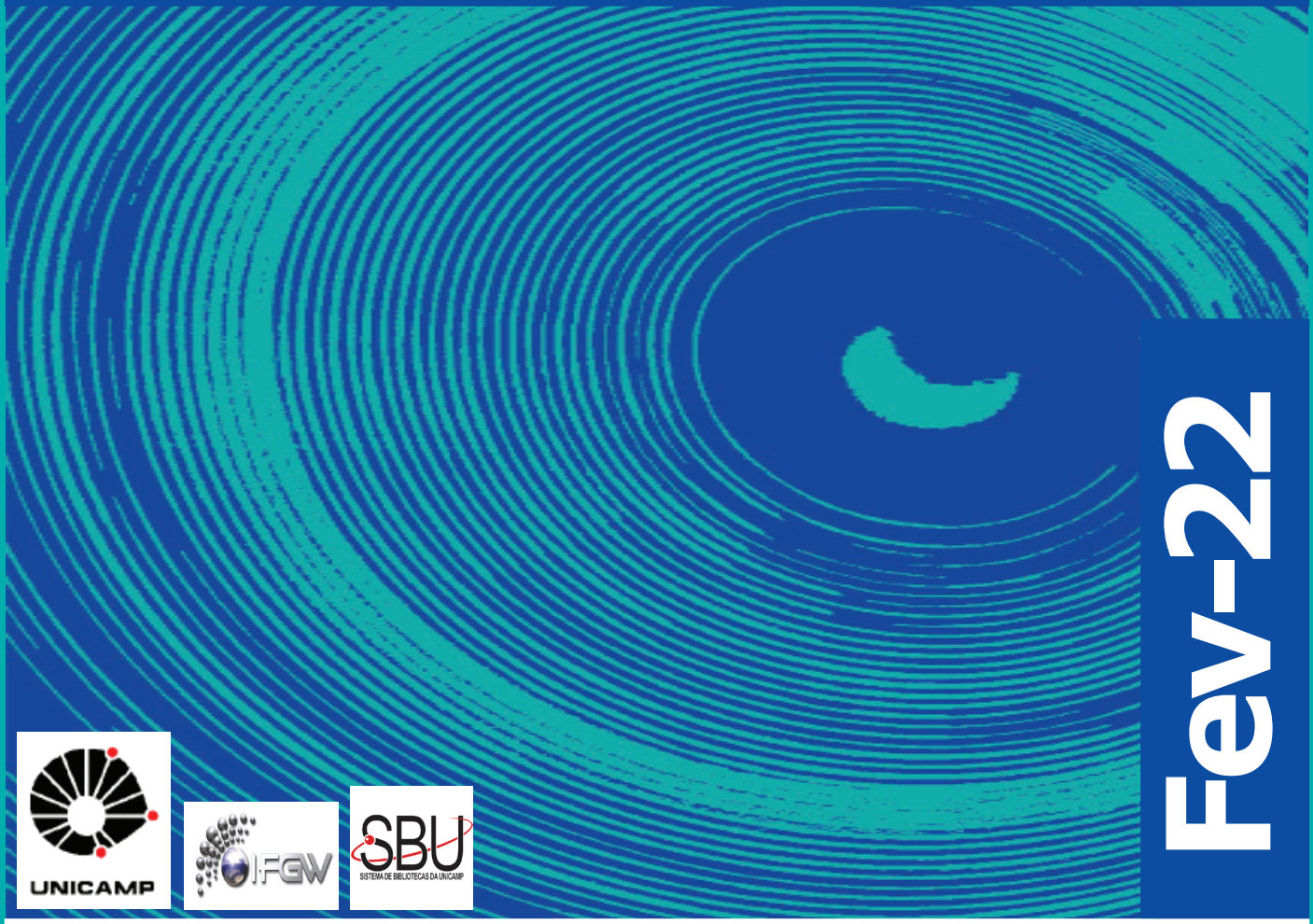

Fev-22

UNICAMP

IFGW

SBU
SISTEMA DE BIBLIOTECAS DA UNICAMP

Artigos publicados 2021 - P328-2021 à P370-2021

Eventos publicados 2021 - P371-2021 à P372-2021

Artigos publicados 2022 - P001-2022 à P033-2022

Aceitos para publicação - A001-2022

Defesas de Dissertações do IFGW - D001-2022 à D002-2022

Defesas de Teses do IFGW - T001-2022 à T003-2022

Artigos publicados 2021

[P328-2021] "A model potential for computing total ionization cross sections of atoms and molecules by electron impact"

Falkowski, A. G.*; Bettega, M. H. F.; **Lima, M. A. P.***; Ferreira, L. G.

We propose a model potential for computing total ionization cross sections for atoms and molecules by electron impact. The potential is obtained by a fitting procedure using the Binary--Encounter-Bethe model cross sections as a starting point. We present total ionization cross section for hydrogen, carbon, nitrogen and oxygen atoms and for hydrogen, nitrogen, water, methane and benzene molecules. The results obtained with our model potential are compared with results obtained with the Binary-Encounter-Bethe model and with the first Born approximation, and agreement is quite good. Our results show that this potential could be used to account for the ionization channel in an electron-molecule collision calculation.

EUROPEAN PHYSICAL JOURNAL D 75[12], 308, 2021. DOI: 10.1140/epjd/s10053-021-00323-0

[P329-2021] "A Review on the Development of Metal Grids for the Upscaling of Perovskite Solar Cells and Modules"

Silva, J. M. C. da; **Goncalves, A. D.*; Marques, F. C.*;** Freitas, J. N. de

Lab-scale perovskite solar cells have reached efficiencies as high as the best monocrystalline silicon cells, with expectations that their manufacturing costs could be lower than those of currently commercialized cells. As a result, efforts are now directed to the production of these cells. In this sense, the use of frontal metal grids in large-area perovskite cells and parallel-connected modules is imperative due to the low conductivity of the transparent conductive substrate usually employed in these devices. For the insertion of grids, a trade-off between reduced resistive losses and the increase in shadowed area must be achieved. Assessment of grid parameters is of utmost importance for the assembly of viable large-scale cells and modules. Furthermore, a direct transfer from grid parameters previously specified for other photovoltaic technologies might not be the best option for perovskite cells. Nonetheless, investigations of grids specifically designed for these cells are still scarce in the literature. Here, grid design, both in terms of metal composition and geometric factors, is discussed, including their development for tandem cells and flexible devices. To provide further insights into the maturity level of this technology, a patent analysis regarding grid designs for perovskite modules is also presented in this review.

SOLAR RRL, Número do artigo: 2100865, 2021. DOI: 10.1002/solr.202100865

[P330-2021] "A(c)(+) Production and Baryon-to-Meson Ratios in pp and p-Pb Collisions at root S-NN=5.02 TeV at the LHC"

Acharya, S.; Aamova, D.; Adler, A.; **Albuquerque, D. S. D.*; Chinellato, D. D.*; Takahashi, J.***; et al. ALICE Collaboration

The prompt production of the charm baryon Lambda(c+) and the A(c)(+)/D-0 production ratios were measured at midrapidity with the ALICE detector in pp and (p)-Pb collisions at root S-NN = 5.02 TeV. These new measurements show a clear decrease of the Lambda(+)(c)/D-0 ratio with increasing transverse momentum (p(T)) in both collision systems in the range 2 < P-T < 12 GeV/c, exhibiting similarities with the light-flavor baryon-tomeson ratios p/pi and Lambda/K-S(0). At low p(T), predictions that include additional color-reconnection mechanisms beyond the leading-color approximation, assume the existence of additional higher-mass charm-baryon states, or include hadronization via coalescence can describe the data, while predictions driven by charmquark fragmentation processes measured in e(+) e(-) and e(-) p collisions significantly underestimate the data. The results presented in this Letter provide significant evidence that the established assumption of universality (colliding-system independence) of parton-to-hadron fragmentation is not sufficient to describe charm-baryon production in hadronic collisions at LHC energies.

PHYSICAL REVIEW LETTERS 127[20], 202301, 2021. DOI: 10.1103/PhysRevLett.127.202301

[P331-2021] "Advances in the study of supercooled water"

Gallo, P.; Bachler, J.; Bove, L. E.; Bohmer, R.; Camisasca, G.; Coronas, L. E.; Corti, H. R.; **Ribeiro, I. D.*; Koning, M. de***; Franzese, G.; Fuentes-Landete, V.; Gainaru, C.; Loerting, T; Oca, J. M. M. de; Poole, P. H.; Rovere, M.; Sciortino, F.; Tonauer, C. M.; Appignanesi, G. A.

In this review, we report recent progress in the field of supercooled water. Due to its uniqueness, water presents numerous anomalies with respect to most simple liquids, showing polyamorphism both in the liquid and in the glassy state. We first describe the thermodynamic scenarios hypothesized for the supercooled region and in particular among them the liquid--liquid critical point scenario that has so far received more experimental evidence. We then review the most recent structural indicators, the two-state model picture of water, and the importance of cooperative effects related to the fact that water is a hydrogen-bonded network liquid. We show throughout the review that water's peculiar properties come into play also when water is in solution, confined, and close to biological molecules. Concerning dynamics, upon mild supercooling water behaves as a fragile glass former following the mode coupling theory, and it turns into a strong glass former upon further cooling. Connections between the slow dynamics and the thermodynamics are discussed. The translational relaxation times of density fluctuations show in fact the fragile-to-strong crossover connected to the thermodynamics arising from the existence of two liquids. When considering also rotations, additional crossovers come to play. Mobility-viscosity decoupling is also discussed in supercooled water and aqueous solutions. Finally, the polyamorphism of glassy water is considered through experimental and simulation results both in bulk and in salty aqueous solutions. Grains and grain boundaries are also discussed.

EUROPEAN PHYSICAL JOURNAL E 44[11], 143, 2021. DOI: 10.1140/epje/s10189-021-00139-1

[P332-2021] "Angle-Resolved Hollow-Core Fiber-Based Curvature Sensing Approach"

Guimaraes, W. M.; **Cordeiro, C. M. B.***; Franco, M. A. R.; **Osorio, J. H.***

We propose and theoretically study a new hollow-core fiber--based curvature sensing approach with the capability of detecting both curvature radius and angle. The new sensing method relies on a tubular-lattice fiber that encompasses, in its microstructure, tubes with three different thicknesses. By adequately choosing the placement of the tubes within the fiber cross-section, and by exploring the spectral shifts of the fiber transmitted spectrum due to the curvature-induced mode field distributions' displacements, we demonstrate a multi-axis curvature sensing method. In the proposed platform, curvature radii and angles are retrieved via a suitable calibration routine, which is based on conveniently adjusting empirical functions to the fiber response.

Evaluation of the sensing method performance for selected cases allowed the curvature radii and angles to be determined with percentual errors of less than 7%. The approach proposed herein provides a promising path for the accomplishment of new curvature sensors able to resolve both the curvature radius and angle.

FIBERS 9[11], 72, 2021. DOI: 10.3390/fib9110072

[P333-2021] "Anisotropic nematic fluctuations above the ferroquadrupolar transition in TmVO4"

Wang, Z.; Vinograd, I.; Mei, Z.; **Menegasso, P.***; Garcia, D.; Massat, P.; Fisher, I. R.; Curro, N. J.

Ferroquadrupole order of local atomic orbitals provides a specific realization of electronic nematic order. TmVO4 is an insulator and undergoes ferroquadrupolar order associated with the local Tm 4 f orbitals at T-Q = 2.15 K. The material is a model system to study nematic order and the roles played by nematic fluctuations. Here we present V-51 nuclear magnetic resonance data as a function of field orientation in a single crystal. Although the spectra are well understood in terms of direct dipolar hyperfine couplings, the spin-lattice relaxation rate exhibits strong anisotropy that cannot be understood in terms of magnetic fluctuations. We find that the spin-lattice relaxation rate scales with the shear elastic constant associated with the ferroquadrupole phase transition, suggesting that quadrupole (nematic) fluctuations dominate the spin-lattice relaxation for in-plane fields.

PHYSICAL REVIEW B 104[20], 205137, 2021. DOI: 10.1103/PhysRevB.104.205137

[P334-2021] "Azimuthally asymmetric tubular lattice hollow-core optical fiber"

Cordeiro, C. M. B.*; Osorio, J. H.*; Guimaraes, W. M.; Franco, M. A. R.

A new, to the best of our knowledge, hollow-core optical fiber based on a tube lattice geometry is proposed. The fiber cross section is formed by eight tubes with five different thicknesses, and the guidance mechanism is based on the inhibited coupling phenomenon. As such, its transmittance spectrum displays low-loss windows intercalated with high-loss regions, each of the latter related to specific core-cladding modal couplings. The spectral behavior of the straight and bent waveguide is numerically analyzed. Simulations on different curvature radii and directions (angles) show the core mode displacement toward the outer side of the curvature and its impact on the spectral shift of the high-loss wavelengths. The different response of each tube resonance is investigated and discussed. The proposed structure identifies a new and promising path for the development of directional curvature sensors.

JOURNAL OF THE OPTICAL SOCIETY OF AMERICA B-OPTICAL PHYSICS 38[12], F23-F28, 2021. DOI: 10.1364/JOSAB.435630

[P335-2021] "Complexity reduction in the 3D Kuramoto model"

Barioni, A. E. D.*; Aguiar, M. A. M. de*

The dynamics of large systems of coupled oscillators is a subject of increasing importance with prominent applications in several areas such as physics and biology. The Kuramoto model, where a set of oscillators move around a circle representing their phases, is a paradigm in this field, exhibiting a continuous transition between disordered and synchronous motion. Reinterpreting the oscillators as rotating unit vectors, the model was extended to higher dimensions by allowing vectors to move on the surface of D-dimensional spheres, with D = 2 corresponding to the original model. It was shown that the transition to synchronous dynamics was discontinuous for odd D. Inspired by results in 2D, Ott et al proposed an ansatz for the density function describing the oscillators and derived equations for the ansatz parameters, effectively reducing the dynamics complexity. Here we take a different approach for the 3D system and construct an ansatz based on spherical harmonics decomposition of the distribution function. Our result differs from Ott's work and leads to similar but simpler equations determining the dynamics of the order parameter. We derive the phase diagram of equilibrium solutions for several distributions of natural frequencies and find excellent agreement with numerical solutions for the full system dynamics. We believe our approach can be generalized to higher dimensions, leading to complexity reduction in other systems of coupled equations.

CHAOS SOLITONS & FRACTALS 149, 111090, 2021. DOI: 10.1016/j.chaos.2021.111090

[P336-2021] "Controlled spatial organization of bacterial growth reveals key role of cell filamentation preceding Xylella fastidiosa biofilm formation"

Anbumani, S.*; Silva, A. M. da*; Carvalho, I. G. B.; Fischer, E. R.; Silva, M. D. E. de S.; **von Zuben, A. A. G.***; Carvalho, H. F.; Souza, A. A. de; Janissen, R.; **Cotta, M. A.***

The morphological plasticity of bacteria to form filamentous cells commonly represents an adaptive strategy induced by stresses. In contrast, for diverse human and plant pathogens, filamentous cells have been recently observed during biofilm formation, but their functions and triggering mechanisms remain unclear. To experimentally identify the underlying function and hypothesized cell communication triggers of such cell morphogenesis, spatially controlled cell patterning is pivotal. Here, we demonstrate highly selective cell adhesion of the biofilm-forming phytopathogen Xylella fastidiosa to gold-patterned SiO2 substrates with well-defined geometries and dimensions. The consequent control of both cell density and distances between cell clusters demonstrated that filamentous cell formation depends on cell cluster density, and their ability to interconnect neighboring cell clusters is distance-dependent. This process allows the creation of large interconnected cell clusters that form the structural framework for macroscale biofilms. The addition of diffusible signaling molecules from supernatant extracts provides evidence that cell filamentation is induced by quorum sensing. These findings and our innovative platform could facilitate therapeutic developments targeting biofilm formation mechanisms of X. fastidiosa and other pathogens.

NPJ BIOFILMS AND MICROBIOMES 7[1], 86, 2021. DOI: 10.1038/s41522-021-00258-9

[P337-2021] "COVID-19 transmission risk factors"

Notari, A.; **Torrieri, G.***

We analyze risk factors correlated with the initial transmission growth rate of the recent COVID-19 pandemic in different countries. The number of cases follows in its early stages an almost exponential expansion; we chose as a starting point in each country the first day d, with 30 cases and we fitted for 12 days, capturing thus the early exponential growth. We looked then for linear correlations of the exponents a with other variables, for a sample of 126 countries. We find a positive correlation, i.e. faster spread of COVID-19, with high confidence level with the following variables, with respective p-value: low Temperature (4.10(-7)), high ratio of old vs. working-age people (3.10(-6)), life expectancy (8.10(-6)), number of international tourists (1.10(-5)), earlier epidemic starting date d, (2.10(-5)),

high level of physical contact in greeting habits (6.10(-5)), lung cancer prevalence (6.10(-5)), obesity in males (1.10(-4)), share of population in urban areas (2.10(-4)), cancer prevalence (3.10(-4)), alcohol consumption (0.0019), daily smoking prevalence (0.0036), and UV index (0.004, 73 countries). We also find a correlation with low Vitamin D serum levels (0.002 - 0.006), but on a smaller sample, similar to 50 countries, to be confirmed on a larger sample. There is highly significant correlation also with blood types: positive correlation with types RH- (3.10(-5)) and A+ (3.10(-3)), negative correlation with B+ (2.10(-4)). We also find positive correlation with moderate confidence level (p-value of 0.02 similar to 0.03) with: CO2/SO emissions, type-1 diabetes in children, low vaccination coverage for Tuberculosis (BCG). Several of the above variables are correlated with each other, and so they are likely to have common interpretations. We thus performed a Principal Component Analysis, to find the significant independent linear combinations of such variables. The variables with loadings of at least 0.3 on the significant PCA are: greeting habits, urbanization, epidemic starting date, number of international tourists, temperature, lung cancer, smoking, and obesity in males. We also analyzed the possible existence of a bias: countries with low GDP-per capita might have less intense testing, and we discuss correlation with the above variables.

PATHOGENS AND GLOBAL HEALTH, Early Access: DEC 2021. DOI: 10.1080/20477724.2021.1993676

[P338-2021] "Charged-particle multiplicity fluctuations in Pb-Pb collisions at root s(NN)=2.76 TeV"

Acharya, S.; Adamova, D.; Adler, A.; **Chinellato, D. D.*; Guardiano, G. G.*; Jahnke, C.*; Takahashi, J.***; et al. ALICE Collaboration

Measurements of event-by-event fluctuations of charged-particle multiplicities in Pb-Pb collisions at root s(NN) = 2.76 TeV using the ALICE detector at the CERN Large Hadron Collider (LHC) are presented in the pseudorapidity range |eta| < 0.8 and transverse momentum 0.2 < p(T) < 2.0 GeV/c. The amplitude of the fluctuations is expressed in terms of the variance normalized by the mean of themultiplicity distribution. The. and p(T) dependences of the fluctuations and their evolution with respect to collision centrality are investigated. The multiplicity fluctuations tend to decrease from peripheral to central collisions. The results are compared to those obtained from HIJING and AMPT Monte Carlo event generators as well as to experimental data at lower collision energies. Additionally, the measured multiplicity fluctuations are discussed in the context of the isothermal compressibility of the high-density strongly-interacting system formed in central Pb-Pb collisions.

EUROPEAN PHYSICAL JOURNAL C 81[11, 1012, 2021. DOI: 10.1140/epjc/s10052-021-09784-4

[P339-2021] "Dark Energy Survey Year 3 Results: Galaxy mock catalogs for BAO analysis"

Ferrero, I.; Crocce, M.; Tutusaus, I.; **Brandao-Souza, A.***; DES Collaboration

The calibration and validation of scientific analysis in simulations is a fundamental tool to ensure unbiased and robust results in observational cosmology. In particular, mock galaxy catalogs are a crucial resource to achieve these goals in the measurement of baryon acoustic oscillation (BAO) in the clustering of galaxies. Here we present a set of 1952 galaxy mock catalogs designed to mimic the Dark Energy Survey Year 3 BAO sample over its full photometric redshift range 0.6x2004;z(photo)N-body simulations of full-sky light cones and were created by populating halos with galaxies, using a hybrid halo occupation distribution - halo abundance matching model. This model has ten free parameters, which were determined, for the first time, using an automatic likelihood minimization procedure. We also introduced a novel technique to assign photometric redshift for simulated galaxies, following a two--dimensional probability distribution with VIMOS Public Extragalactic Redshift Survey data. The calibration was designed to match the observed abundance of galaxies as a function of photometric redshift, the distribution of photometric redshift errors, and the clustering amplitude on scales smaller than those used for BAO measurements. An exhaustive analysis was done to ensure that the mocks reproduce the input properties. Finally, mocks were tested by comparing the angular correlation function w(theta), angular power spectrum C-l, and projected clustering xi(p)(r(perpendicular to)) to theoretical predictions and data. The impact of volume replication in the estimate of the covariance is also investigated. The success in accurately reproducing the photometric redshift uncertainties and the galaxy clustering as a function of redshift render this mock creation pipeline as a benchmark for future analyses of photometric galaxy surveys.

ASTRONOMY & ASTROPHYSICS 656, A106, 2021. DOI: 10.1051/0004-6361/202141744

[P340-2021] "Diverging Quantum Speed Limits: A Herald of Classicality"

Poggi, P. M.; Campbell, S.; **Deffner, S.***

When is the quantum speed limit (QSL) really quantum? While vanishing QSL times often indicate emergent classical behavior, it is still not entirely understood what precise aspects of classicality are at the origin of this dynamical feature. Here, we show that vanishing QSL times (or, equivalently, diverging quantum speeds) can be traced back to reduced uncertainty in quantum observables and can thus be understood as a consequence of emerging classicality for these particular observables. We illustrate this mechanism by developing a QSL formalism for continuous-variable quantum systems undergoing general Gaussian dynamics. For these systems, we show that three typical scenarios leading to vanishing QSL times, namely large squeezing, small effective Planck's constant, and large particle number, can be fundamentally connected to each other. In contrast, by studying the dynamics of open quantum systems and mixed states, we show that the classicality that emerges due to incoherent mixing of states from the addition of classical noise typically increases the QSL time.

PRX QUANTUM 2[4], 040349, 2021. DOI: 10.1103/PRXQuantum.2.040349

[P341-2021] "Electronic excitation of benzene by low energy electron impact and the role of higher lying Rydberg states"

Falkowski, A. G.*; Costa, R. F. da; Kossoski, F.; Brunger, M. J.; **Lima, M. A. P.***

Benzene is undoubtedly one of the most studied target molecules in electron scattering experiments and calculations. However, there is still a huge knowledge gap on the electronic excitation cross sections of this fundamental collision. Here, we report calculated differential and integral cross sections for elastic and electronic excitation, as well as total cross sections, for electron scattering by the benzene molecule, for impact energies in the 10-50 eV range. We have employed the Schwinger multichannel method, in two levels of approximation. By including extra diffuse functions in the second calculation, the role of higher lying Rydberg states in the multichannel coupling scheme was assessed. We found that such states have minor effects on the elastic and total cross sections. In contrast, the electronic excitation cross sections of the

lower-lying bands decrease in magnitude when accounting for the higher Rydberg states, and this effect becomes more pronounced at lower impact energies. Our computed elastic cross sections are in quite good agreement with the available experimental data, whereas the comparison for the electronic excitation channels is still satisfactory. We also discuss the need for accurate excitation energies in order to properly compare theoretical and experimental electronic excitation cross sections.

EUROPEAN PHYSICAL JOURNAL D 75[12], 310, 2021. DOI: 10.1140/epjd/s10053-021-00326-x

[P342-2021] "Emerging two-dimensional tellurides"

Siddique, S.; Gowda, C. C.; Demiss, S.; **Tromer, R.***; Paul, S.; Sadasivuni, K. K.; Olu, E. F.; Chandra, A.; Kochat, V.; **Galvao, D. S.***; Kumbhakar, P.; Mishra, R.; Ajayan, P. M.; Tiwary, C. S.

Two-dimensional (2D) materials are at the forefront of current materials research due to their exciting and unique properties. 2D tellurides are emerging materials which are yet to be fully explored. To provide an overview of this emergent field, in this review, we discuss the structure, properties, synthesis methods, and applications of selected 2D tellurides, with stoichiometry of MxTey, and MxNyTez, (M, N are metal atoms). We present a summary of the latest advances in modeling, experimental synthesis, and characterization of 2D tellurides. Additionally, stress and strain-induced tunability of the physical properties have been reviewed, with a focus on the application of 2D tellurides in electronic, optoelectronic, and magnetic devices. We have discussed many emergent quantum properties of these materials. Finally, we conclude with a perspective on the future of 2D metal tellurides.

MATERIALS TODAY 51, 402-426, 2021. DOI: 10.1016/j.mattod.2021.08.008

[P343-2021] "Energetic cost of Hamiltonian quantum gates"

Deffner, S.*

Landauer's principle laid the main foundation for the development of modern thermodynamics of information. However, in its original inception the principle relies on semiformal arguments and dissipative dynamics. Hence, if and how Landauer's principle applies to unitary quantum computing is less than obvious. Here, we prove an inequality bounding the change of Shannon information encoded in the logical quantum states by quantifying the energetic cost of Hamiltonian gate operations. The utility of this bound is demonstrated by outlining how it can be applied to identify energetically optimal quantum gates in theory and experiment. The analysis is concluded by discussing the energetic cost of quantum error correcting codes with non-interacting qubits, such as Shor's code.

EPL 134[4], 40002, 2021. DOI: 10.1209/0295-5075/134/40002

[P344-2021] "Environment-Assisted Shortcuts to Adiabaticity"

Touil, A.; **Deffner, S.***

Envariance is a symmetry exhibited by correlated quantum systems. Inspired by this "quantum fact of life, " we propose a novel method for shortcuts to adiabaticity, which enables the system to evolve through the adiabatic manifold at all times, solely by controlling the environment. As the main results, we construct the unique form of the driving on the environment that enables such dynamics, for a family of composite states of arbitrary dimension. We compare the cost of this environment-assisted technique with that of counterdiabatic driving, and we illustrate our results for a two-qubit model.

ENTROPY 23[11], 1479, 2021. DOI: 10.3390/e23111479

[P345-2021] "In Vivo and In Vitro Taste Assessment of Artesunate-Mefloquine, Praziquantel, and Benznidazole Drugs for Neglected Tropical Diseases and Pediatric Patients"

Boniatti, J.; Tappin, M. R. R.; Teixeira, R. G. D. da S.; Gandos, T. D. V.; Rios, L. P. S.; Ferreira, I. A. M.; Oliveira, K. C.; Calil-Elias, S.; Santana, A. K. M.; Fonseca, L. B. da; **Shimizu, F. M.***; Carr, O.; Oliveira Junior, O. N.; Dantas, F. M. L.; Amendoeira, F. C.; Vicosa, A. L.

The assessment of drug taste is crucial for pediatric treatments so that formulations can be developed to enhance their effectiveness. In this study, in vivo and in vitro methods were applied to evaluate the taste of tablets of three drugs administered to children without taste-masking excipients to treat tropical diseases, namely artesunate-mefloquine (ASMQ), praziquantel (PZQ), and benznidazole (BNZ). In the first method, a model of rat palatability was adapted with recirculation to ensure sample dispersion, and the data were analyzed using ANOVA (single factor, 95%). The taste assessment results (in vivo) indicated an aversion to the three medicines, denoted by the animals retracting themselves to the bottom of the box after the first contact with the drugs. For the placebo samples, the animals behaved normally, indicating that taste perception was acceptable. The second method was based on the in vitro analysis of capacitance data from a homemade impedimetric electronic tongue. Consistent with the in vivo taste assessment results, the data points obtained with PZQ, ASMQ, and BNZ were far away from those of their placebos in a map built with the multidimensional projection technique referred to as Interactive Document Mapping (IDMAP). A combined analysis of the results with the two methods allowed us to confirm the bitterness of the three drugs, also pointing to electronic tongues as a promising tool to replace in vivo palatability tests.

AAPS PHARMSCITECH 23[1], 22, 2021. DOI: 10.1208/s12249-021-02162-z

[P346-2021] "Inclusive J/psi production at midrapidity in pp collisions at root s=13 Tev"

Acharya, S.; Adamova, D.; **Chinellato, D. D.*; Guardiano, G. G.*; Jahnke, C.*; Takahashi, J.***; et al. ALICE Collaboration

We report on the inclusive J/psi production cross section measured at the CERN Large Hadron Collider in proton-proton collisions at a center-of-mass energy root s = 13 TeV. The J/psi mesons are reconstructed in the e(+)e(-) decay channel and the measurements are performed at midrapidity (vertical bar y vertical bar < 0.9) in the transverse-momentum interval 0 < p(T) < 40 GeV/c, using a minimum-bias data sample corresponding to an integrated luminosity L-int = 32.2 nb(-1) and an Electromagnetic Calorimeter triggered data sample with L-int = 8.3 pb(-1). The p(T)-integrated J/psi production cross section at midrapidity, computed using the minimumbias data sample, is d sigma/dy vertical bar(y) =0 = 8.97 +/- 0.24 (stat) 0.48 (syst) +/- 0.15 (lumi) mu b. An approximate logarithmic dependence with the collision energy is suggested by these results and available world data, in agreement with model predictions. The integrated and p(T)-differential measurements are compared with measurements in pp collisions at lower energies and with several recent phenomenological calculations based on the non-relativistic QCD and Color Evaporation models.

EUROPEAN PHYSICAL JOURNAL C 81[12], 1121, 2021. DOI: 10.1140/epjc/s10052-021-09873-4

[P347-2021] "KinesiOS: A Telerehabilitation and Functional Analysis System for Post-Stroke Physical Rehabilitation Therapies?"

Scudeletti, L. R.; **Brandao, A. F.***; Dias, D. R. C.; Brega, J. R. F.

The stroke (also known as a Cerebrovascular Accident) is one of the medical conditions that most kills and incapacitates people in the world, affecting men, women and children of many different age brackets. Studies have been presented in recent years addressing the use of systems for motion capture in post stroke rehabilitation, showing that these tools could be just as efficient as the more traditional methods. In this study, we shall present KinesiOS, a system for telerehabilitation and recognition of movements for the motor and neurofunctional assessment of patients who are undergoing rehabilitation. The system tracks the joints in the human body based on their respective spatial coordinates, and then using the obtained data to construct a guide to movements in the form of a virtual skeleton, while measuring the amplitude of the movements (also known as a Range of Motion) within a certain motor action and showing the results in real time. The tracking of the joints is carried out using a Microsoft Kinect (R) sensor v2, while data processing, we used the C# programming language. We created the visualizations using the Windows Presentation Foundation (R) technology, and the data was saved in a cloud structure using the MongoDB (R) database. Preliminary tests performed on six healthy volunteers showed the efficiency of the system for the calculation of amplitude of movements, enabling data analysis in real time and through telemonitoring. KinesiOS is an alternative tool, portable and low-cost, compared with the traditional systems based on tracking of joints.

COMPUTATIONAL SCIENCE AND ITS APPLICATIONS, ICCSA 2021, PT II, Book Series: Lecture Notes in Computer Science, Volume: 12950, p. 174-185, 2021. DOI: 10.1007/978-3-030-86960-1_13

[P348-2021] "Magnetic nanoparticles in biomedical applications: A review"

Materon, E. M.; Miyazaki, C. M.; Carr, O.; Joshi, N.; Picciani, P. H. S.; Dalmaschio, C. J.; Davis, F.; **Shimizu, F. M.***

Biomedical applications with emphasis on the design of smart materials, specifically magnetic nanoparticles (MNPs) are considered to have technological benefits because they can be manipulated using magnetic fields. Magnetic NPs have been widely used in hyperthermia, target drug delivery system, imaging, and extraction of biomolecules, postulating them also as an important tool in cancer treatment. Morphological structures of magnetic materials have drawn tremendous attention from diverse scientific fields due to their unique surface chemistry, nontoxicity, biocompatibility, and particularly their inducible magnetic moment. This review features recent research accomplishments made in the biomedical field using magnetic nanoparticles. The first part gives a comprehensive overview of magnetic nanoparticles in the treatment of chronic diseases and drug targeting. The second part includes the role of magnetic nanoparticles in electrochemical, optical-based immunoassays. The review also outlines the current challenges and future research perspectives for fostering advanced and high-performance magnetic nanoparticles in technological applications.

APPLIED SURFACE SCIENCE ADVANCES 6, 100163, 2021. DOI: 10.1016/j.apsadv.2021.100163

[P349-2021] "Magnetic Vortex Domain Wall Observation on Polycrystalline Imperfect Iron-Cobalt Alloy Nanowires Growing on 1050 Aluminum"

Londono-Calderon, C. L.; Londono-Calderon, A.; Moscoso-Londono, O.; Galindo, A.; Ponce, A.; Pampillo, L. G.; Martinez--Garcia, R.; Yacaman, M. J.; **Knobel, M.***

Herein, the magnetic vortex domain wall structure of polycrystalline imperfect iron-cobalt alloy nanowires (Nws) growing on 1050 aluminum by pulsed electrodeposition is reported. The magnetic properties are analyzed using magnetometry and off-axis electron holography. The electrodeposited Nw arrays show homogeneous elemental composition and exhibit a structure composed of piled-up grains of small crystallites. The saturation magnetization, coercive field, and reduced remanence, measured in directions parallel and perpendicular to the Nw's axis, are studied as a function of the temperature. Although the array of Nws on anodized aluminum grows both straight and within an inclination angle, in both cases, a high shape anisotropy is noticed, which is the most predominant contribution to the magnetic behavior. Misalignments and defects of the Nws in the array, as well as the wide distribution of lengths and diameters, do not contribute significantly to coercivity dispersion. A modified model is used to explain the changes in the magnetic behavior of the Nw's arrays, which accounts for structural imperfections and magnetostatic interactions. The reversal magnetization arising from the vortex domain wall propagation via localized curling is verified by off-axis electron holography.

PHYSICA STATUS SOLIDI A-APPLICATIONS AND MATERIALS SCIENCE, Número do artigo: 2100265, 2021. DOI: 10.1002/pssa.202100265

[P350-2021] "Measurement of differential t(t)over-bar production cross sections in the full kinematic range using lepton plus jets events from proton-proton collisions at root s=13 TeV"

Tumasyan, A.; Adam, W.; **Chinellato, J. A.***; et al. CMS Collaboration

Measurements of differential and double-differential cross sections of top-quark pair (t (t) over bar) production arc presented in the lepton + jets channels with a single electron or muon and jets in the final state. The analysis combines for the first time signatures of top quarks with low transverse momentum p(T), where the top-quark decay products can be identified as separated jets and isolated leptons, and with high p(T), where the decay products are collimated and overlap. The measurements arc based on proton-proton collision data at is - = 13 TeV collected by the CMS experiment at the LHC, corresponding to an integrated luminosity of 137 fb(-1). The cross sections are presented at the parton and particle levels, where the latter minimizes extrapolations based on theoretical assumptions. Most of the measured differential cross sections are well described by standard model predictions with the exception of some double-differential distributions. The inclusive t (t) over bar production cross section is measured to be sigma(t (t) over bar) = 791 +/- 25 pb, which constitutes the most precise measurement in the lepton + jets channel to date.

PHYSICAL REVIEW D 104[9], 092013, 2021. DOI: 10.1103/PhysRevD.104.092013

[P351-2021] "Measurement of prompt open-charm production cross sections in proton-proton collisions at root s=13 TeV"

Tumasyan, A.; Adam, W.; Ambrogi, F.; **Chinellato, J. A.*; Tonelli Manganote, E. J.***; et al. CMS Collaboration

The production cross sections for prompt open-charm mesons in proton-proton collisions at a center-of-mass energy of 13TeV are reported. The measurement is performed using a data sample collected by the CMS experiment corresponding to an integrated luminosity of 29 nb(-1).

The differential production cross sections of the D*(+/-), D-+/-, and D-0 ((D) over bar (0)) mesons are presented in ranges of transverse momentum and pseudorapidity 4 < p(T) < 100 GeV and vertical bar eta vertical bar < 2.1, respectively. The results are compared to several theoretical calculations and to previous measurements.

JOURNAL OF HIGH ENERGY PHYSICS [11], 225, 2021. DOI: 10.1007/JHEP11(2021)225

[P352-2021] "Measurement of the inclusive and differential t(t)over-bar gamma cross sections in the single-lepton channel and EFT interpretation at root s=13 TeV"

Tumasyan, A.; Adam, W.; **Chinellato, J. A.***; et al. CMS Collaboration

The production cross section of a top quark pair in association with a photon is measured in proton-proton collisions at a center-of-mass energy of 13 TeV. The data set, corresponding to an integrated luminosity of 137 fb(-1), was recorded by the CMS experiment during the 2016-2018 data taking of the LHC. The measurements are performed in a fiducial volume defined at the particle level. Events with an isolated, highly energetic lepton, at least three jets from the hadronization of quarks, among which at least one is b tagged, and one isolated photon are selected. The inclusive fiducial t (t) over bar'gamma cross section, for a photon with transverse momentum greater than 20 GeV and pseudorapidity vertical bar eta vertical bar< 1.4442, is measured to be 798 +/- 7(stat) +/- 48(syst) fb, in good agreement with the prediction from the standard model at next-to-leading order in quantum chromodynamics. The differential cross sections are also measured as a function of several kinematic observables and interpreted in the framework of the standard model effective field theory (EFT), leading to the most stringent direct limits to date on anomalous electromagnetic dipole moment interactions of the top quark and the photon.

JOURNAL OF HIGH ENERGY PHYSICS [12], 180, 2021. DOI: 10.1007/JHEP12(2021)180

[P353-2021] "Measurement of the top quark mass using events with a single reconstructed top quark in pp collisions at root s=13 TeV"

Tumasyan, A.; Adam, W.; **Chinellato, J. A.***; et al. CMS Collaboration

A measurement of the top quark mass is performed using a data sample enriched with single top quark events produced in the t channel. The study is based on protonproton collision data, corresponding to an integrated luminosity of 35.9 fb(-1), recorded at root s = 13TeV by the CMS experiment at the LHC in 2016. Candidate events are selected by requiring an isolated high-momentum lepton (muon or electron) and exactly two jets, of which one is identified as originating from a bottom quark. Multivariate discriminants are designed to separate the signal from the background. Optimized thresholds are placed on the discriminant outputs to obtain an event sample with high signal purity. The top quark mass is found to be 172.13(-0.77)(+0.76) GeV, where the uncertainty includes both the statistical and systematic components, reaching sub-GeV precision for the first time in this event topology. The masses of the top quark and antiquark are also determined separately using the lepton charge in the final state, from which the mass ratio and difference are determined to be 0.9952(-0.0104)(+0.0079) and 0.83(-1.35)(+1.79) GeV, respectively. The results are consistent with CPT invariance.

JOURNAL OF HIGH ENERGY PHYSICS [12], 161, 2021. DOI: 10.1007/JHEP12(2021)161

[P354-2021] "Measurements of the Electroweak Diboson Production Cross Sections in Proton-Proton Collisions at root s=5.02 TeV Using Leptonic Decays"

Tumasyan, A.; Adam, W.; **Chinellato, J. A.***; et al. CMS Collaboration

The first measurements of diboson production cross sections in proton-proton interactions at a center-of-mass energy of 5.02 TeV are reported. They are based on data collected with the CMS detector at the LHC, corresponding to an integrated luminosity of 302 pb(-1). Events with two, three, or four charged light leptons (electrons or muons) in the final state are analyzed. The WW, WZ, and ZZ total cross sections are measured as sigma(WW) = 37:0(-5.2)(+5.5) (stat)(-2.6)(+2.7) (syst) pb, sigma(WZ) = 6.4(-2.1)(+2.5) (stat)(-0.3)(+0.5)(syst) pb, and sigma(ZZ) = 5.3(-2.1)(+2.5)(stat)(-0.4)(+0.5) (syst) pb. All measurements are in good agreement with theoretical calculations at combined next-to-next-to-leading order quantum chromodynamics and next-to-leading order electroweak accuracy.

PHYSICAL REVIEW LETTERS 127[9], 191801, 2021. DOI: 10.1103/PhysRevLett.127.191801

[P355-2021] "Metabolic Volume Measurements in Multiple Myeloma"

Takahashi, M. E. S.*; Lorand-Metze, I.; Souza, C. A. de; Mesquita, C. T.; Fernandes, F. A.; Carvalheira, J. B. C.; Ramos, C. D.

Multiple myeloma (MM) accounts for 10-15% of all hematologic malignancies, as well as 20% of deaths related to hematologic malignant tumors, predominantly affecting bone and bone marrow. Positron emission tomography/computed tomography with 18F-fluorodeoxyglucose (FDG-PET/CT) is an important method to assess the tumor burden of these patients. It is often challenging to classify the extent of disease involvement in the PET scans for many of these patients because both focal and diffuse bone lesions may coexist, with varying degrees of FDG uptake. Different metrics involving volumetric parameters and texture features have been proposed to objectively assess these images. Here, we review some metabolic parameters that can be extracted from FDG-PET/CT images of MM patients, including technical aspects and predicting MM outcome impact. Metabolic tumor volume (MTV) and total lesion glycolysis (TLG) are volumetric parameters known to be independent predictors of MM outcome. However, they have not been adopted in clinical practice due to the lack of measuring standards. CT--based segmentation allows automated, and therefore reproducible, calculation of bone metabolic metrics in patients with MM, such as maximum, mean and standard deviation of the standardized uptake values (SUV) for the entire skeleton. Intensity of bone involvement (IBI) is a new parameter that also takes advantage of this approach with promising results. Other indirect parameters obtained from FDG-PET/CT images, such as visceral adipose tissue glucose uptake and subcutaneous adipose tissue radiodensity, may also be useful to evaluate the prognosis of MM patients. Furthermore, the use and quantification of new radiotracers can address different metabolic aspects of MM and may have important prognostic implications.

METABOLITES 11[12], 875, 2021. DOI: 10.3390/metabo11120875

[P356-2021] "Motor imagery practice and feedback effects on functional connectivity"

Stefano Filho, C. A.*; Attux, R.*; Castellano, G.*

Objective. The use of motor imagery (MI) in motor rehabilitation protocols has been increasingly investigated as a potential technique for enhancing traditional treatments, yielding better clinical outcomes. However, since MI performance can be challenging, practice is usually required. This demands appropriate training, actively engaging the MI-related brain areas, consequently enabling the user to properly benefit from it. The role of feedback is central for MI practice. Yet, assessing which underlying neural changes are feedback-specific or purely due to MI practice is still a challenging effort, mainly due to the difficulty in isolating their contributions. In this work, we aimed to assess functional connectivity (FC) changes following MI practice that are either extrinsic or specific to feedback. Approach. To achieve this, we investigated FC, using graph theory, in electroencephalography (EEG) and functional magnetic resonance imaging (fMRI) data, during MI performance and at resting-state (rs), respectively. Thirty healthy subjects were divided into three groups, receiving no feedback (control), 'false' feedback (sham) or actual neurofeedback (active). Participants underwent 12-13 hands-MI EEG sessions and pre- and post-MI training fMRI exams. Main results. Following MI practice, control participants presented significant increases in degree and in eigenvector centrality for occipital nodes at rs-fMRI scans, whereas sham-feedback produced similar effects, but to a lesser extent. Therefore, MI practice, by itself, seems to stimulate visual information processing mechanisms that become apparent during basal brain activity. Additionally, only the active group displayed decreases in inter-subject FC patterns, both during MI performance and at rs-fMRI. Significance. Hence, actual neurofeedback impacted FC by disrupting common inter-subject patterns, suggesting that subject-specific neural plasticity mechanisms become important. Future studies should consider this when designing experimental NFBT protocols and analyses.

JOURNAL OF NEURAL ENGINEERING 18[6], 066048, 2021. DOI: 10.1088/1741-2552/ac456d

[P357-2021] "NiVCe-Layered Double Hydroxide as Multifunctional Nanomaterials for Energy and Sensor Applications

Goncalves, J. M.; Lima, I. S.; Azeredo, N. F. B.; Rocha, D. P.; **Siervo, A. de***; Angnes, L.

Multifunctional nanomaterials have been attracting increasing attention as solutions to the existing challenges in energy systems and sensing technologies. In this regard, multifunctional NiVCe-layered double hydroxide (NiVCe-LDH) nanoparticles were synthesized by the modified sol-gel method. The analysis of this material demonstrated excellent potential for its utilization as electrode materials for hybrid supercapacitor, oxygen evolution reaction (OER), and sensor applications. The NiVCe-LDH nanoparticles delivered a specific charge of 740 C g(-1) at 10 A g(-1) and decent rate performance (charge retention of 68.7% at 100 A g(-1)), showing excellent prospects as electrode material for hybrid energy storage devices. In addition, NiVCe-LDH nanoparticles have also been successfully applied as a proof-of-concept for OER, as confirmed by their low Tafel slope of 47 mV dec(-1). Finally, trimetallic NiVCe-LDH-based screen-printed electrodes were developed for the sensing of hydrogen peroxide directly in a real complex mouthwash sample, achieving a satisfactory recovery value of around 98% using a fast and simple batch injection analysis procedure. These results allow us to predict the great potential of this trimetallic hydroxide for building electrochemical sensors with good perspectives as electroactive material for OER processes and energy storage technologies.

FRONTIERS IN MATERIALS 8, 781900, 2021. DOI: 10.3389/fmats.2021.781900

[P358-2021] "Observation of tW production in the single--lepton channel in pp collisions at root s=13 TeV"

Tumasyan, A.; Adam, W.; **Chinellato, J. A.***; et al. CMS Collaboration

A measurement of the cross section of the associated production of a single top quark and a W boson in final states with a muon or electron and jets in proton-proton collisions at root s = 13 TeV is presented. The data correspond to an integrated luminosity of 36 fb(-1) collected with the CMS detector at the CERN LHC in 2016. A boosted decision tree is used to separate the tW signal from the dominant t (t) over bar background, whilst the subleading W+jets and multijet backgrounds are constrained using data-based estimates. This result is the first observation of the tW process in final states containing a muon or electron and jets, with a significance exceeding 5 standard deviations. The cross section is determined to be 89 +/- 4 (stat) +/- 12 (syst) pb, consistent with the standard model.

JOURNAL OF HIGH ENERGY PHYSICS [11], 111, 2021. DOI: 10.1007/JHEP11(2021)111

[P359-2021] "Probing effective field theory operators in the associated production of top quarks with a Z boson in multilepton final states at root s=13 TeV"

Tonon, N.; Petersen, H. A.; Martin, M. A.; **Chinellato, J. A.***; et al. CMS Collaboration

A search for new top quark interactions is performed within the framework of an effective field theory using the associated production of either one or two top quarks with a Z boson in multilepton final states. The data sample corresponds to an integrated luminosity of 138 fb(-1) of proton-proton collisions at root s = 13 TeV collected by the CMS experiment at the LHC. Five dimension-six operators modifying the electroweak interactions of the top quark are considered. Novel machine-learning techniques are used to enhance the sensitivity to effects arising from these operators. Distributions used for the signal extraction are parameterized in terms of Wilson coefficients describing the interaction strengths of the operators. All five Wilson coefficients are simultaneously fit to data and 95% confidence level intervals are computed. All results are consistent with the SM expectations.

JOURNAL OF HIGH ENERGY PHYSICS [12], 083, 2021. DOI: 10.1007/JHEP12(2021)083

[P360-2021] "Reagentless and sub-minute laser-scribing treatment to produce enhanced disposable electrochemical sensors via additive manufacture"

Rocha, D. P.; Ataide, V. N.; **Siervo, A. de***; Gonsalves, J. M.; Munoz, R. A. A.; Paixa, T. R. L. C.; Angnes, L.

3D printing is the most popular form of additive manufacturing, and conductive 3D-printed platforms have been recognized as an emerging class of devices with high potential for electrochemistry. Nevertheless, as-printed electrodes provide poor conductivity due to the presence of high amounts of insulating thermoplastic material, requiring surface post--treatments to enhance their electrochemical performance. Such treatments often employ non-eco-friendly, costly, and time-consuming protocols. In this regard, we propose, for the first time, a sub-minute (around 50 s) and reagentless surface treatment of carbon-black/PLA-based 3D-printed electrodes using a Photo-Thermal approach by a CO2 laser. After the proposed treatment (optimized conditions: the power of 6.2%, the scan rate of 20 mm s-1, and height of 10 mm), a marked improvement in the electrochemical electrode response (current increase and peak-to-peak separation) was achieved towards the detection of catechol, ascorbic and uric acids, paracetamol, hexaammineruthenium(III) chloride, and Ferri/ferrocyanide redox couple.

The enhanced simultaneous determination of Cd2+, Pb2+, and Cu2+ was also demonstrated. As a proof-ofconcept, the quantification of the adulterant paracetamol in a real seized cocaine sample was performed using a fully 3D-printed electrochemical system, and a good recovery value of 97.8% was acquired. To explain all the improved results, the electrode was carefully characterized by imaging, spectroscopic and electrochemical techniques. Additionally, the between--measurement % relative standard deviation (%RSD) was 6.8% (n = 12), while the between-device %RSD was 7.5% (n = 6) at the 1 mu mol L-1 paracetamol, indicating adequate manufacturing reproducibility. Thus, the strategies developed here open up new possibilities for applications of carbon--based 3D-printed electrodes in analytical electrochemistry.

CHEMICAL ENGINEERING JOURNAL 425, 130594, 2021. DOI: 10.1016/j.cej.2021.130594

[P361-2021] "Sample Concentration Affects Optical Gain Results in Colloidal Nanomaterials: Circumventing the Distortions by Below Band Gap Excitation"

Nagamine, G.*; Ferreira, T. A. C.*; Almeida, D. B.*; Lemus, J. C.*; Chang, J. H.; Jeong, B. G.; Bae, W. K.; **Padilha, L. A.***

Ultrafast spectroscopy studies have been key to the development of optical materials, including colloidal semiconductor nanocrystals (NCs) engineered for lighting and light-harvesting technologies. Several physical processes, which are revealed by ultrafast spectroscopy in NCs, are highly dependent on the average number of excitons created per NC, including optical gain properties and multiexciton interactions. Consequently, proper considerations regarding NC populations are necessary to avoid misinterpretations. In this paper, we present an experimental and theoretical analysis of the influence of the sample optical density (OD) at the excitation energy on the results of ultrafast spectroscopy studies in NCs. We show that the pump beam depletion caused by high ODs can drastically change the results from transient absorption (TA) experiments leading to data misinter-pretations, such as the overestimation of the optical gain threshold. Based on that, we propose a robust modification on the TA technique, which allows for an OD-independent characterization, free of distortions. The modification consists of pumping the sample below its band gap energy, limiting the electronic excitation to a two-photon absorption process, resulting in an effectively zero OD for the pump beam and a uniform excitation in the direction of the beam propagation. Consequently, an undistorted TA signal is produced, allowing for precise characterization of NCs, including the gain/absorption cross section, gain coefficient, and gain threshold. Furthermore, the uniform excitation allows for higher signal--to-noise ratio, independent of the sample concentration.

ACS PHOTONICS, Early Access Date: DEC 2021. DOI: 10.1021/acsphotonics.1c01293

[P362-2021] "Search for a heavy resonance decaying to a top quark and a W boson at root s=13 TeV in the fully hadronic final state"

Tumasyan, A.; Adam, W.; **Chinellato, J. A.***; et al. CMS Collaboration

A search for a heavy resonance decaying to a top quark and a W boson in the fully hadronic final state is presented. The analysis is performed using data from proton--proton collisions at a center-of-mass energy of 13 TeV, corresponding to an integrated luminosity of 137 fb(-1) recorded by the CMS experiment at the LHC. The search is focused on heavy resonances, where the decay products of each top quark or W boson are expected to be reconstructed as a single, large-radius jet with a distinct substructure. The production of an excited bottom quark, b*, is used as a benchmark when setting limits on the cross section for a heavy resonance decaying to a top quark and a W boson. The hypotheses of b* quarks with left-handed, right-handed, and vector-like chiralities are excluded at 95% confidence level for masses below 2.6, 2.8, and 3.1 TeV, respectively. These are the most stringent limits on the b* quark mass to date, extending the previous best limits by almost a factor of two.

JOURNAL OF HIGH ENERGY PHYSICS [12], 106, 2021. DOI: 10.1007/JHEP12(2021)106

[P363-2021] "Search for Long-Lived Particles Decaying in the CMS End Cap Muon Detectors in Proton-Proton Collisions at root s=13 TeV"

Tumasyan, A.; Adam, W.; **Chinellato, J. A.***; et al. CMS Collaboration

A search for long-lived particles (LLPs) produced in decays of standard model (SM) Higgs bosons is presented. The data sample consists of 137 fb(-1) of proton-proton collisions at root s = 13 TeV, recorded at the LHC in 2016-2018. A novel technique is employed to reconstruct decays of LLPs in the end cap muon detectors. The search is sensitive to a broad range of LLP decay modes and to masses as low as a few GeV. No excess of events above the SM background is observed. The most stringent limits to date on the branching fraction of the Higgs boson to LLPs subsequently decaying to quarks and tau(+) tau(-) are found for proper decay lengths greater than 6, 20, and 40 m, for LLP masses of 7, 15, and 40 GeV, respectively.

PHYSICAL REVIEW LETTERS 127[26], 261804, 2021. DOI: 10.1103/PhysRevLett.127.261804

[P364-2021] "Search for new particles in events with energetic jets and large missing transverse momentum in proton-proton collisions at root s=13 TeV"

Tumasyan, A.; Adam, W.; **Chinellato, J. A.***; et al. CMS Collaboration

A search is presented for new particles produced at the LHC in proton-proton collisions at root s = 13 TeV, using events with energetic jets and large missing transverse momentum. The analysis is based on a data sample corresponding to an integrated luminosity of 101 fb(-1), collected in 2017-2018 with the CMS detector. Machine learning techniques are used to define separate categories for events with narrow jets from initial--state radiation and events with large-radius jets consistent with a hadronic decay of a W or Z boson. A statistical combination is made with an earlier search based on a data sample of 36 fb(-1), collected in 2016. No significant excess of events is observed with respect to the standard model background expectation determined from control samples in data. The results are interpreted in terms of limits on the branching fraction of an invisible decay of the Higgs boson, as well as constraints on simplified models of dark matter, on first-generation scalar leptoquarks decaying to quarks and neutrinos, and on models with large extra dimensions. Several of the new limits, specifically for spin-1 dark matter mediators, pseudoscalar mediators, colored mediators, and leptoquarks, are the most restrictive to date.

JOURNAL OF HIGH ENERGY PHYSICS [11], 153, 2021. DOI: 10.1007/JHEP11(2021)153

[P365-2021] "Single Diameter Modulation Effects on Ni Nanowire Array Magnetization Reversal"

Arzuza, L. C. C.*; Vega, V.; Prida, V. M.; Moura, K. O.; **Pirota, K. R.*; Beron, F.***

Geometrically modulated magnetic nanowires are a simple yet efficient strategy to modify the magnetic domain wall propagation since a simple diameter modulation can achieve its pinning during the nanowire magnetization reversal. However, in dense systems of parallel nanowires, the stray fields arising at the diameter interface can interfere with the domain wall propagation in the neighboring nanowires. Therefore, the magnetic behavior of diameter-modulated nanowire arrays can be quite complex and depending on both short and long-range interaction fields, as well as the nanowire geometric dimensions. We applied the first-order reversal curve (FORC) method to bi-segmented Ni nanowire arrays varying the wide segment (45-65 nm diameter, 2.5-10.0 mu m length). The FORC results indicate a magnetic behavior modification depending on its length/diameter aspect ratio. The distributions either exhibit a strong extension along the coercivity axis or a main distribution finishing by a fork feature, whereas the extension greatly reduces in amplitude. With the help of micromagnetic simulations, we propose that a low aspect ratio stabilizes pinned domain walls at the diameter modulation during the magnetization reversal. In this case, long-range axial interaction fields nucleate a domain wall at the nanowire extremities, while short-range ones could induce a nucleation at the diameter interface. However, regardless of the wide segment aspect ratio, the magnetization reversal is governed by the local radial stray fields of the modulation near null magnetization. Our findings demonstrate the capacity of distinguishing between complex magnetic behaviors involving convoluted interaction fields.

NANOMATERIALS 11[12], 3403, 2021. DOI: 10.3390/nano11123403

[P366-2021] "Structural and spectroscopic investigation of the charge-ordered, short-range ordered, and disordered phases of the Co3O2BO3 ludwigite"

Galdino, C. W.*; Freitas, D. C.; Medrano, C. P. C.; Sanchez, D. R.; **Tartaglia, R.***; Rabello, L. P.; Mendonca, A. A.; Ghivelder, L.; Continentino, M. A.; Zapata, M. J. M.; Pinheiro, C. B.; Azevedo, G. M.; Rodriguez-Velamazan, J. A.; Garbarino, G.; Nunez-Regueiro, M.; **Granado, E.***

Charge ordering is prone to occur in crystalline materials with mixed-valence ions. It is presumably accompanied by a structural phase transition, with possible exceptions in compounds that already present more than one inequivalent site for the mixed-valence ions in the charge-disordered phase. In this work, we investigate the representative case of the homometallic Co ludwigite Co2+2Co3+O2BO3 (Pbam space group) with four distinct Co crystallographic sites [M1-M 4] surrounded by oxygen octahedra. The mixed-valent character of the Co ions up to at least T = 873 K is verified through x-ray absorption near-edge structure (XANES) experiments. Single crystal x-ray diffraction (XRD) and neutron powder diffraction (NPD) confirm that the Co ions at the M4 site are much smaller than the others at low temperatures, consistent with a Co3+ oxidation state at M4 and Co2+ at the remaining sites. The size difference between the Co ions in the M4 and M2 sites is continuously reduced upon warming above approximate to 370 K, indicating a gradual charge redistribution within the M4-M2-M 4 (424) ladder in the average structure. Minor structural anomalies with no space group modification are observed near 475 and 495 K, where sharp phase transitions were previously revealed by calorimetry and electrical resistivity data. An increasing structural disorder, beyond a conventional thermal effect, is noted above approximate to 370 K, manifested by an anomalous increment of XRD Debye-Waller factors and broadened vibrational modes observed by Raman scattering. The local Co-O distance distribution, revealed by Co K-edge extended x-ray absorption fine structure (EXAFS) data and analyzed with an evolutionary algorithm method, is similar to that inferred from the XRD crystal structure below approximate to 370 K. At higher temperatures, the local Co-O distance distribution remains similar to that found at low temperatures, at variance with the average crystal structure obtained with XRD. We conclude that the oxidation states Co2+ and Co3+ are instantaneously well defined in a local atomic level at all temperatures, however the thermal energy promotes local defects in the charge-ordered configuration of the 424 ladders upon warming. These defects coalesce into a phase-segregated state within a narrow temperature interval (475 < T < 495 K). Finally, a transition at approximate to 500 K revealed by differential scanning calorimetry (DSC) in the iron ludwigite Fe3O2BO3 is discussed.

PHYSICAL REVIEW B 104[19], 195151, 2021. DOI: 10.1103/PhysRevB.104.195151

[P367-2021] "Synthesis, characterization, and incorporation of upconverting nanoparticles into a dental adhesive"

Pacheco, R. R.; Garcia-Flores, A. F.; Soto-Montero, J. R.; **Lesseux, G. G.*; Lancelotti, A. C. R. A.*; Martinez, E. D.*; Rettori, C.*; Urbano, R. R.***; Rueggeberg, F. A.; Giannini, M.

The purpose of this study was to describe the synthesis, characterization, and functionalization of b-NaYF4:30%Yb/0.5%Tm upconverting nanocrystals for use as nanofillers in a dental adhesive and microscopically evaluate the interface between the particles and a commercial adhesive. The upconverting nanoparticles were synthesized and purified by thermal decomposition, and their chemical composition determined by energy dispersive X-Ray spectroscopy. The crystalline structure was characterized using X-Ray diffraction and morphology and size were observed with scanning and transmission electron microscopy. Upconverting emission was evaluated by spectrophotometry irradiating the particles with a 975 nm diode laser. Particles were functionalized with polyacrylic acid and the success was confirmed by measurement of Zeta Potential and transmission electron microscopy. The results of X-ray diffraction found a pure hexagonal phase crystalline pattern. Scanning electron microscopy showed uniform dispersion of hexagonal-shaped particles of approximately 150 nm. Upconversion emission was observed in 344 nm, 361 nm, 450 nm, 474nm, 646 nm, 803 nm. Functionalization success was confirmed by formation of a stable aqueous colloid with a Zeta potential of -29.5mV and the absence of voids in the particle-adhesive interface on the transmission electron microscopy images. The reported synthesis and functionalization process produced upconverting nanoparticles emitting photons within the blue spectral region (450 nm and 474 nm).

BRAZILIAN ORAL RESEARCH 35, e120, 2021. DOI: 10.1590/1807-3107bor-2021.vol35.0120

[P368-2021] "Technical note: MC-GPU breast dosimetry validations with other Monte Carlo codes and phase space file implementation"

Massera, R. T.*; Thomson, R. M.; **Tomal, A.***

Purpose To validate the MC-GPU Monte Carlo (MC) code for dosimetric studies in X-ray breast imaging modalities: mammography, digital breast tomosynthesis, contrast enhanced digital mammography, and breast-CT. Moreover, to implement and validate a phase space file generation routine. Methods The MC-GPU code (v. 1.5 DBT) was modified in order to generate phase space files and to be compatible with PENELOPE v. 2018 derived cross-section database. Simulations were performed with homogeneous and anthropomorphic breast phantoms for different breast imaging techniques. The glandular dose was computed for each case and compared with results from the PENELOPE (v. 2014) + penEasy (v. 2015) and egs_brachy (EGSnrc) MC codes.

Afterward, several phase space files were generated with MC--GPU and the scored photon spectra were compared between the codes. The phase space files generated in MC-GPU were used in PENELOPE and EGSnrc to calculate the glandular dose, and compared with the original dose scored in MC-GPU. Results MC-GPU showed good agreement with the other codes when calculating the glandular dose distribution for mammography, mean glandular dose for digital breast tomosynthesis, and normalized glandular dose for breast-CT. The latter case showed average/maximum relative differences of 2.3%/27%, respectively, compared to other literature works, with the larger differences observed at low energies (around 10 keV). The recorded photon spectra entering a voxel were similar (within statistical uncertainties) between the three MC codes. Finally, the reconstructed glandular dose in a voxel from a phase space file differs by less than 0.65%, with an average of 0.18%-0.22% between the different MC codes, agreement within approximately 2 sigma statistical uncertainties. In some scenarios, the simulations performed in MC-GPU were from 20 up to 40 times faster than those performed by PENELOPE. Conclusions The results indicate that MC-GPU code is suitable for breast dosimetric studies for different X-ray breast imaging modalities, with the advantage of a high performance derived from GPUs. The phase space file implementation was validated and is compatible with the IAEA standard, allowing multiscale MC simulations with a combination of CPU and GPU codes.

MEDICAL PHYSICS 49[1], 244-253, 2021. DOI: 10.1002/mp.15342

[P369-2021] "The texture of collagen in the microenvironments of Merkel cell carcinoma"

Laurito, T. L.; Franca, F. T.; Vieira-Damiani, G.; **Pelegati, V. B.*; Baratti, M. O.*; Carvalho, H. F. de*; Cesar, C. L.***; Moraes, A. M. de; Cintra, M. L.; Teixeira, F.

Solid tumors typically contain high levels of fibrillar collagen. The increased stromal collagen deposition usually promotes cancer progression since biochemical and biophysical cues from tumor-associated collagen fibers stimulate neoplastic cells. Few studies have investigated the relationship between Merkel cell carcinoma (MCC) and the extracellular matrix (ECM), but there are no works evaluating collagen. This is an observational, analytical, retrospective study including 11 patients with MCC. Primary tumor-stained sections were evaluated by second harmonic generation microscopy and texture analysis. Peritumoral texture features (area fraction, mean gray value, entropy, and contrast) showed much lower values than normal skin (P < .0001) revealing extensively altered structure of peritumoral collagen fibers. These differences were not significant between tumors with unfavorable and favorable known prognostic factors. Profound changes in collagen fibers present in the stroma accompanying primary MCC may contribute to the aggressive behavior of this tumor. Our results indicate that whatever MCC histological subtype, size or anatomical location, MCC promotes the same type of ECM for its development. As an outlook, therapies using ECM macromolecules or fibroblasts (the architects of ECM remodeling) as target could be useful in the treatment of MCC.

MEDICINE 100[47], e27925, 2021. DOI: 10.1097/MD.0000000000027925

[P370-2021] "Thermodynamic Analyses on Nanoarchitectonics of Perovskite from Lead Iodide: Arrhenius Activation Energy"

Borrero, N. F. V.*; Silva, J. M. C. da*; Coutinho, N. F.*; Freitas, J. N.; **Marques, F. C.***

Amongst the different perovskites being investigated for application in solar cells, one of the most frequently scrutinized is methylammonium lead iodide CH3NH3PbI3 (or MAPbI(3)), which is usually obtained by the reaction of lead iodide (PbI2) with methylammonium iodide (MAI). Although this perovskite has been extensively studied and utilized in the manufacture of high-efficiency solar cells, its formation chemistry is still not well understood. Reliable experimental determination of the activation energy between PbI2 and MAI has been difficult due to the rapid reaction at room temperature. In this work, we determined the activation energy by adopting the Arrhenius equation. This was possible by controlling the reaction using MAI vapor, instead of liquid solution. This procedure allowed the reaction to be carried out at temperatures of up to 150 degrees C. The formation of MAPbI(3) films was obtained by a two-step process: deposition of thin PbI2 film by thermal evaporation and subsequent conversion into perovskite by exposure to MAI vapor. The conversion of PbI2 to MAPbI(3) as a function of temperature was probed by X-ray diffraction. An activation energy of 0.12 +/- 0.02 eV was obtained. This low value explains the ease of MAPbI(3) formation at low temperatures, and partially explains its instability in environmental conditions.

JOURNAL OF INORGANIC AND ORGANOMETALLIC POLYMERS AND MATERIALS, Early Access: DEC 2021, DOI: 10.1007/s10904-021-02169-w

Eventos publicados 2021

[P371-2021] "Imaging with a Rigid Multimode Fiber Bundle"

Pellegrini, P. E. S.; Biazoli, C. R.; **Jarschel, P. F.***; Panepucci, R. R.; Gabrielli, L. H.; IEEE

A rigid multimode fiber bundle is proposed for imaging, in an experimental setup with no interferometric measurements. The great amount of propagating modes in the fiber bundle, along with its high numerical aperture, enable us to set predetermined focus targets with, approximately, 60 mu m resolution. In order to do so, an optimization process to build transmission matrices was applied to overcome modal interference and obtain focus. Here, we also show that transmission matrices could be stored and combined, so focus could be simultaneously achieved in different locations, at the distal end of the fiber bundle.

SBFoton International Optics and Photonics Conference (SBFoton IOPC), MAY 31-JUN 02, 2021, ELECTR NETWORK. Article Number: 1570708021, 2021. DOI: 10.1109/SBFOTONIOPC50774.2021.9461957

[P372-2021] "Synchrotron infrared nanospectroscopy as a game changer in nanophotonics"

Mayer, R. A.*; Feres, F. H.*; Freitas, R. O.; IEEE

Modern technological applications share a variety of common demands, especially the need for smaller functional devices operating with unprecedented data processing power. Hence, nanoscale devices for light traffic are promising candidates for that end. Therefore, a set of advances are required to drive research into real-world applications in this area, including disruptive advances in the available characterization tools. This work presents an overview on how synchrotron infrared nanospectroscopy has contributed to the progress of nanophotonics. Technique description, data processing, and recent studies highlight the uniqueness of the technique for accessing nano-optical phenomena in novel quantum materials.

SBFoton International Optics and Photonics Conference (SBFoton IOPC), MAY 31-JUN 02, 2021, ELECTR NETWORK, Article Number: 1570720903, 2021. DOI: 10.1109/SBFOTONIOPC50774.2021.9461984

Artigos publicados 2022

[P001-2022] "Actual, sham and no-feedback effects in motor imagery practice"

Stefano filho, C. A.*; Attux, R.; **Castellano, G.***

Motor imagery (MI) has been associated to clinical benefits for motor and cognitive rehabilitation protocols through the appropriate identification and training of its corresponding neural patterns. Although potentially impactful factors for MI practice have been identified, issues regarding system feedback and the underlying neurophysiological alterations such practice can produce still remain. In this work, we investigated how feedback can affect the outcome of a MI practice protocol with a brain-computer interface (BCI), when providing: no feedback, sham feedback or actual neurofeedback. We assessed whether event-related desynchronization occurrence (EO) and classification accuracy (CA) varied in each scenario. We found that: (i) practice without feedback did not enhance either metric; (ii) sham feedback yielded a wider variety of outcomes than for the control group, but no statistical significance was observed at the group level; (iii) although users trained to adapt to the BCI classifier, improvements in CA and both contra and ipsilateral EO were observed for the neurofeedback group: average CA increased from (71.3 +/- 3.7) % to (75.5 +/- 5.8) %, whereas median EO increased approximately 5% per session This study reinforces the relevance of neurofeedback in MI learning and provides new insights into neurophysiological correlates throughout the practice protocol. We also hint at a possible placebo effect that provides significant correlations between EO and CA only for the sham group.

BIOMEDICAL SIGNAL PROCESSING AND CONTROL 71, 103262, Part: B, 2022. DOI: 10.1016/j.bspc.2021.103262

[P002-2022] "All-optical real-time monitoring of air/vacuum valves in water pipeline systems using fiber Bragg gratings"

Aquino, G. A. de; De Lucca, Y. D. L.; **Cabral, T. D.*; Lazari, P. M.*;** Martim, A. L. S. S.; Fujiwara, E.; **Cordeiro, C. M. B.***; Dalfre, J. G.

A novel strategy for online real-time remote monitoring of air/vacuum valves in water pipelines is proposed and validated. The sensing setup consists of a fiber Bragg grating operating as an optical strain gauge and embedded into a 3D-printed thermoplastic polyurethane casing, which is then fixed to the intake/exhaust port of an air/vacuum valve and allowed to bend in response to the airflow. Experimentation with a test bench simulating water adductor piping systems shows that the proposed strategy can detect and discriminate between air purge and intake events, measure their duration, and possibly quantify the volume of displaced air. The proposed all-optical setup was compared against an orifice plate approach, producing consistent results while being more compact, robust, reliable, and requiring a single fiber optic sensor to achieve all measurements, as opposed to the four or up electronic pressure sensors with the orifice plate.

JOURNAL OF THE BRAZILIAN SOCIETY OF MECHANICAL SCIENCES AND ENGINEERING 44[1], 5, 2022. DOI: 10.1007/s40430-021-03310-z

[P003-2022] "Charm-quark fragmentation fractions and production cross section at mid rapidity in pp collisions at the LHC"

Acharya, S.; Adamova, D.; **Chinellato, D. D.*; Guardiano, G. G.*; Jahnke, C.*; Takahashi, J.***; et al. ALICE Collaboration

Recent p(T)-integrated cross-section measurements of the ground-state charm mesons and baryons, D-0, D+, D-s(+), Lambda(+)(c), and Xi(0)(c) are used to evaluate the charm fragmentation fractions and production cross section per unit of rapidity at midrapidity (vertical bar y vertical bar < 0.5), in pp collisions at root s = 5.02 TeV at the LHC. The latter is d sigma(c<(c)over) (bar>)/dy vertical bar(vertical bar y vertical bar<0.5) = 1165 +/- 44(stat)(-101)(+131) (syst) mu b. These measurements were obtained for the first time in hadronic collisions at the LHC, including the charm baryon states, recently measured by ALICE at midrapidity. The charm fragmentation fractions differ significantly from the values measured in e(+)e(-) and ep collisions, providing evidence of the dependence of the parton-to-hadron fragmentation fractions on the collision system, indicating that the assumption of their universality is not supported by the measured cross sections. An increase of a factor of about 3.3 for the fragmentation fraction for the Lambda(+)(c) with a significance of 5 sigma between the values obtained in pp collisions and those obtained in e(+) e(-) (ep) collisions is reported. The fragmentation fraction for the Xi(0)(c) was obtained for the first time in any collision system. The measured fragmentation fractions were used to update the c (c) over bar cross sections per unit of rapidity at vertical bar y vertical bar < 0.5 at root s = 2.76 and 7 TeV, which are about 40% higher than the previously published results. The data were compared with perturbative-QCD calculations and lie at the upper edge of the theoretical bands.

PHYSICAL REVIEW D 105[1], L011103, 2022. DOI: 10.1103/PhysRevD.105.L011103

[P004-2022] "Cubic to hexagonal tuning in Fe2Mn(Si1-xGex) Heusler alloys"

Pimentel, B.; **Andrade, V. M.***; Paula, V. G. de; **Pirota, K. R.*; Beron, F.***; Cardoso, M. A.; Goncalves, J. N.; Amaral, J. S.; Santos, A. M. dos; Reis, M. S.

The competition between the stability of the cubic and hexagonal full Heusler alloys and the implications concerning their magnetic properties were systematically studied through the detailed structural and magnetic characterization of the Fe2Mn(Si1-xGex) system. This system was specifically chosen as the parent compositions are cubic (x = 0) and hexagonal (x = 1). It is found that the formation of hexagonal phases occurs for the x >= 0.6 samples, whereas its phase fraction monotonically increases with x until the pure hexagonal Fe2MnGe is formed. The change in structure results in high sensitiveness of both the saturation of magnetization (MS) and Curie temperature (TC) with x values, related to a strong magnetocrystalline anisotropy of the hexagonal phase. Both cubic and hexagonal magnetic features were qualitatively reproduced by Density Functional Theory (DFT) calculations. This work provides an experimental and theoretical foundation for further design of Heusler systems with controlled structures and magnetic properties.

JOURNAL OF ALLOYS AND COMPOUNDS 893, 162236, 2022. DOI: 10.1016/j.jallcom.2021.162236

[P005-2022] "Dark Energy Survey Year 3 results: galaxy sample for BAO measurement"

Rosell, A. C.; Rodriguez-Monroy, M.; **Brandao-Souza, A.***; et al. DES Collaboration

In this paper, we present and validate the galaxy sample used for the analysis of the baryon acoustic oscillation (BAO) signal in the Dark Energy Survey (DES) Y3 data. The definition is based on a colour and redshift-dependent magnitude cut optimized to select galaxies at redshifts higher than 0.5, while ensuring a high-quality determination. The sample covers similar to 4100 deg(2) to a depth of i = 22.3 (AB) at 10 sigma. It contains 7031 993 galaxies in the redshift range from z = 0.6 to 1.1, with a mean effective redshift of 0.835. Redshifts are estimated with the machine learning algorithm DNF, and are validated using the VIPERS PDR2 sample. We find a mean redshift bias of z(bi)(as) similar to 0.01 and a mean uncertainty, in units of 1 + z, of sigma(68)similar to 0.03. We evaluate the galaxy population of the sample, showing it is mostly built upon Elliptical to Sbc types. Furthermore, we find a low level of stellar contamination of less than or similar to 4 per cent. We present the method used to mitigate the effect of spurious clustering coming from observing conditions and other large-scale systematics. We apply it to the BAO sample and calculate weights that are used to get a robust estimate of the galaxy clustering signal. This paper is one of a series dedicated to the analysis of the BAO signal in DFS Y3. In the companion papers, we present the galaxy mock catalogues used to calibrate the analysis and the angular diameter distance constraints obtained through the fitting to the BAO scale.

MONTHLY NOTICES OF THE ROYAL ASTRONOMICAL SOCIETY 509[1], 778-799, 2022. DOI: 10.1093/mnras/stab2995

[P006-2022] "Differences in brain activity between fast and slow responses on psychomotor vigilance task: an fNIRS study"

Nogueira, M. G.; Silvestrin, M.; Barreto, C. S. F.; Sato, J. R.; **Mesquita, R. C.***; Biazoli, C.; Baptista, A. F.

Attention is a basic human function underlying every other cognitive process. It is demonstrated in the functional Magnetic Resonance Imaging literature that frontoparietal networks are involved with attentive performance while default mode networks are involved with inattentive performance. Yet, it is still not clear whether similar results would be found with functional Near-Infrared Spectroscopy. The goal of our study was to investigate differences in hemodynamic activity measured by functional Near-Infrared Spectroscopy between fast and slow responses on a simple sustained attention task both before and after stimulus onset. Thirty healthy adults took part in the study. Our results have shown differences between fast and slow responses only on channels over medial frontal cortex and inferior parietal cortex (p < 0,05). These differences were observed both before and after stimulus presentation. It is discussed that functional Near-Infrared Spectroscopy is a good tool to investigate the frontoparietal network and its relationship with performance in attention tasks; it could be used to further investigate other approaches on attention, such as the dual network model of cognitive control and brain states views based on complex systems analysis; and finally, it could be used to investigate attention in naturalistic settings.

BRAIN IMAGING AND BEHAVIOR, Early Access: JAN 2022. DOI: 10.1007/s11682-021-00611-8

[P007-2022] "Effects of virtual reality-based motor rehabilitation: a systematic review of fMRI studies"

Feitosa, J. A.*; Fernandes, C. A.*; Casseb, R. F.; **Castellano, G.***

Background. The use of virtual reality (VR) as a rehabilitation tool has been shown to induce motor and cognitive improvements in different populations. Functional magnetic resonance imaging (fMRI) has been used to investigate neuroplasticity resulting from these treatments. We hypothesize that VR rehabilitation induces functional improvement and brain changes that can be detected by fMRI. Objective. To systematically review the effects of VR intervention on the cortical reorganization measured by fMRI and associated with functional improvement. Approach. We performed a systematic review of studies published between 2005 and 2021. Papers were retrieved from six databases using the following keywords: 'motor rehabilitation', 'fMRI' and 'virtual reality'. Case studies, pre-post studies, cross-sectional studies, and randomized controlled trials published were included. Manuscripts were assessed by The National Institutes of Health study quality assessment tools to determine their quality. Main results. Twenty-three articles met our eligibility criteria: 18 about VR rehabilitation in stroke and five on other clinical conditions (older adults, cerebral palsy, and Parkinson's disease). Changes in neural patterns of activation and reorganization were revealed in both the ipsilesional and the contralesional hemispheres. Results were located mainly in the primary motor cortex, sensorimotor cortex and supplementary motor area in post-stroke patients in the acute, subacute, and chronic rehabilitation phases, and were associated with functional improvement after VR intervention. Similar effects were observed in older adults and in patients with other neurological diseases with improved performance. Significance. Most stroke-related studies showed either restoration to normal or increase of activation patterns or relateralization at/to the ipsilesional hemisphere, with some also reporting a decrease in activity or extent of activation after VR therapy. In general, VR intervention demonstrated evidence of efficacy both in neurological rehabilitation and in performance improvement of older adults, accompanied by fMRI evidence of brain reorganization.

JOURNAL OF NEURAL ENGINEERING 19[1], 011002, 2022. DOI: 10.1088/1741-2552/ac456e

[P008-2022] "Efficient integrated tri-modal coupler for few--mode fibers"

Ruiz, J. L. P.*; Rocha, L. G.; Yang, J.; Kocabas, S. E.; Li, M. J.; Aldaya, I.; Dainese, P.; Gabrielli, L. H.

This paper demonstrates a high-efficiency vertical grating coupler for the LP01x, LP11ax, and LP11bx modes of a graded-index few-mode fiber. The coupler is composed of a non-uniform straight bidirectional grating that was inverse-designed to address the desired fiber modes, combined with two mode-selective directional couplers and two tapers. The device was fabricated by e-beam lithography with a minimum feature size of 100 nm and presented coupling efficiencies of -3.0 dB, -3.6 dB, and -3.4 dB for the LP01x, LP11ax, and LP11bx modes, respectively. The high efficiency of the proposed CMOS-compatible coupler demonstrates its potential as a key device for high-capacity networks exploiting space division multiplexing on few-mode fibers.

OPTICS EXPRESS 30[2], 2539-2546, 2022. DOI: 10.1364/OE.446097

[P009-2022] "Ergotropy from quantum and classical correlations"

Touil, A.; Cakmak, B.; **Deffner, S.***

It is an established fact that quantum coherences have thermodynamic value. The natural question arises, whether other genuine quantum properties such as entanglement can also be exploited to extract thermodynamic work. In the present analysis, we show that the ergotropy can be expressed as a function of the quantum mutual information, which demonstrates the contributions to the extractable work from classical and quantum correlations. More specifically, we analyze bipartite quantum systems with locally thermal states, such that the only contribution to the ergotropy originates in the correlations.

Our findings are illustrated for a two-qubit system collectively coupled to a thermal bath.

JOURNAL OF PHYSICS A-MATHEMATICAL AND THEORETICAL 55[2], 025301, 2022. DOI: 10.1088/1751-8121/ac3eba

[P010-2022] "Exploring smoking-gun signals of the Schwinger mechanism in QCD"

Aguilar, A. C.*; Ferreira, M. N.*; Papavassiliou, J.

In Quantum Chromodynamics, the Schwinger mechanism endows the gluons with an effective mass through the dynamical formation of massless bound-state poles that are longitudinally coupled. The presence of these poles affects profoundly the infrared properties of the interaction vertices, inducing crucial modifications to their fundamental Ward identities. Within this general framework, we present a detailed derivation of the non-Abelian Ward identity obeyed by the pole-free part of the three-gluon vertex in the softgluon limit, and determine the smoking-gun displacement that the onset of the Schwinger mechanism produces to the standard result. Quite importantly, the quantity that describes this distinctive feature coincides formally with the bound-state wave function that controls the massless pole formation. Consequently, this signal may be computed in two independent ways: by solving an approximate version of the pertinent BetheSalpeter integral equation, or by appropriately combining the elements that enter in the aforementioned Ward identity. For the implementation of both methods we employ two- and three-point correlation functions obtained from recent lattice simulations, and a partial derivative of the ghost-gluon kernel, which is computed from the corresponding Schwinger-Dyson equation. Our analysis reveals an excellent coincidence between the results obtained through either method, providing a highly nontrivial self-consistency check for the entire approach. When compared to the null hypothesis, where the Schwinger mechanism is assumed to be inactive, the statistical significance of the resulting signal is estimated to be 3 standard deviations.

PHYSICAL REVIEW D 105[1], 014030, 2022. DOI: 10.1103/PhysRevD.105.014030

[P011-2022] "Fluctuation theorem for irreversible entropy production in electrical conduction"

Bonanca, M. V. S.*; Deffner, S.*

Linear irreversible thermodynamics predicts that the entropy production rate can become negative. We demonstrate this prediction for metals under AC driving whose conductivity is well described by the Drude-Sommerfeld model. We then show that these negative rates are fully compatible with stochastic thermodynamics, namely, that the entropy production does fulfill a fluctuation theorem. The analysis is concluded with the observation that the stochastic entropy production as defined by the surprisal or ignorance of the Shannon information does not agree with the phenomenological approach.

PHYSICAL REVIEW E 105[1], L012105, 2022. DOI: 10.1103/PhysRevE.105.L012105

[P012-2022] "Generalization of the Fission-Track Arrhenius Annealing Equations"

Guedes, S.*; Lixandrao, A. L.*; Hadler, J. C.*

Fission-track annealing models describe the recovery kinetics of a crystalline structure damaged by the interaction with fission fragments during the geological thermal history of a mineral sample. Arrhenius type equations have been successfully applied to model annealing and are at the core of thermal history (temperature, T, as a function of time, t, paths) reconstruction programs for fission-track thermochronology. In this work, the Arrhenius equations are generalized and synthesized in a composite equation that allows for the generation of Arrhenius-type equations by turning on/off parameters and by appropriately choosing functions of ln t and T-1. Geometrical features of the Arrhenius-type equations in the Arrhenius pseudo-space (T-1, ln t) are explored. Three examples of new models for annealing of fission tracks in apatite, obtained from the composite model, are presented, and their extrapolation to the geological timescale is discussed. The presented composite model can be applied to other studies involving annealing experiments, such as the annealing of alpha recoil damage in minerals.

MATHEMATICAL GEOSCIENCES, Early Access: JAN 2022. DOI: 10.1007/s11004-021-09987-1

[P013-2022] "Hyperspectral imaging thermometry assisted by upconverting nanoparticles: Experimental artifacts and accuracy"

Martinez, E. D.; Brites, C. D. S.; **Urbano, R. R.*; Rettori, C.***; Carlos, L. D.

We combined the sensing capabilities of Er3+-doped upconverting nanoparticles (UCNPs) with hyperspectral microscopy to construct thermal images on thermally active nanostructures. Here, we studied the heat dissipation of a percolating network of silver nanowires under controlled electric current flow. We quantified the electrothermal action by analyzing the hyperspectral data and constructing 2D maps for the emission intensity, the signal-to-noise ratio, and the thermometric parameter. By studying selected clusters in the network, we concluded that the temperature is quite uniform across the film without any significant thermal gradients. Nonetheless, the thermal evolution was clearly sensed by the UCNPs when the heat dissipation due to the Joule effect was turned on and off, validating the use of this method for studying slow-dynamic thermal processes. Finally, we discuss the accuracy of the thermal readings and the systematic limitations of the proposed method.

PHYSICA B-CONDENSED MATTER 629, 413639, 2022. DOI: 10.1016/j.physb.2021.413639

[P014-2022] "Imaging the electrostatic landscape of unstrained self-assemble GaAs quantum dots"

Lanzoni, E. M.; Silva, S. F. C. da; Knopper, M. F.; **Garcia, A. J.***; Costa, C. A. R.; **Deneke, C.***

Unstrained GaAs quantum dots are promising candidates for quantum information devices due to their optical properties, but their electronic properties have remained relatively unexplored until now. In this work, we systematically investigate the electronic structure and natural charging of GaAs quantum dots at room temperature using Kelvin probe force microscopy (KPFM). We observe a clear electrical signal from these structures demonstrating a lower surface potential in the middle of the dot. We ascribe this to charge accumulation and confinement inside these structures. Our systematical investigation reveals that the change in surface potential is larger for a nominal dot filling of 2 nm and then starts to decrease for thicker GaAs layers. Using k center dot p calculation, we show that the confinement comes from the band bending due to the surface Fermi level pinning.

We find a correlation between the calculated charge density and the KPFM signal indicating that k center dot p calculations could be used to estimate the KPFM signal for a given structure. Our results suggest that these self-assembled structures could be used to study physical phenomena connected to charged quantum dots like Coulomb blockade or Kondo effect.

NANOTECHNOLOGY 33[16], 165701, 2022. DOI: 10.1088/1361-6528/ac47ce

[P015-2022] "Improving Quantitative EDS Chemical Analysis of Alloy Nanoparticles by PCA Denoising: Part I, Reducing Reconstruction Bias"

Moreira, M.*; Hillenkamp, M.*; Divitini, G.; Tizei, L. H. G.; Ducati, C.; **Cotta, M. A.*; Rodrigues, V.*; Ugarte, D.***

Scanning transmission electron microscopy is a crucial tool for nanoscience, achieving sub-nanometric spatial resolution in both image and spectroscopic studies. This generates large datasets that cannot be analyzed without computational assistance. The so-called machine learning procedures can exploit redundancies and find hidden correlations. Principal component analysis (PCA) is the most popular approach to denoise data by reducing data dimensionality and extracting meaningful information; however, there are many open questions on the accuracy of reconstructions. We have used experiments and simulations to analyze the effect of PCA on quantitative chemical analysis of binary alloy (AuAg) nanoparticles using energy-dispersive X-ray spectroscopy. Our results demonstrate that it is possible to obtain very good fidelity of chemical composition distribution when the signal-to-noise ratio exceeds a certain minimal level. Accurate denoising derives from a complex interplay between redundancy (data matrix size), counting noise, and noiseless data intensity variance (associated with sample chemical composition dispersion). We have suggested several quantitative bias estimators and noise evaluation procedures to help in the analysis and design of experiments. This work demonstrates the high potential of PCA denoising, but it also highlights the limitations and pitfalls that need to be avoided to minimize artifacts and perform reliable quantification.

MICROSCOPY AND MICROANALYSIS, Early Access: JAN 2022. DOI: 10.1017/S1431927621013933

[P016-2022] "Influence of milk proteins on the adhesion and formation of Bacillus sporothermodurans biofilms: Implications for dairy industrial processing"

Alonso, V. P. P.; **Ferreira, R. C. de C.*; Cotta, M. A.*;** Kabuki, D. Y.

Bacillus sporothermodurans is a producer of highly heat-resistant spores, which is a problem for the dairy industry worldwide. In this work, we studied the attachment and biofilm formation on stainless steel surfaces in contact with milk proteins (casein and whey). The results of the biofilm formation were obtained by the plate count method. In conjunction, biofilms (niches and cell sizes) were measured by scanning electron microscopy (SEM) on the 1st, 5th and 10th day. X-ray photoelectron spectroscopy (XPS) was a complementary technique that probed the conditioning of the substrate surface after 24 h. The milk proteins affected the total bacterial count in the samples, and also influenced the biofilm architecture. Sessile cell counts varied from 4.3 log CFU/cm2 in the attachment stage to up to 10.2 log CFU/cm2 in the matured biofilm stage. The spore counts varied from <1.4 +/- 0.02 (1st day) to 3.7 log +/- 1.1 log spores/cm2 (10th day). The control group at the biofilm maturation stage (5th day) had higher niches than at the cell fixation (1st day) and was different from the other groups that showed active dispersion in the presence of milk proteins. The same occurred on the 10th day for the control group. Circular patterns in the biofilm with casein, passive dispersal and elongated cells were also observed. Enzyme treatment and disinfectants may be used to remove or reduce biofilm formation.

FOOD CONTROL 134, 108743, 2022. DOI: 10.1016/j.foodcont.2021.108743

[P017-2022] "Measurement of double-parton scattering in inclusive production of four jets with low transverse momentum in proton-proton collisions at root s=13 TeV"

Tumasyan, A.; Adam, W.; **Chinellato, J. A.***; et al. CMS Collaboration

A measurement of inclusive four-jet production in proton-proton collisions at a center-of-mass energy of 13 TeV is presented. The transverse momenta of jets within vertical bar eta vertical bar 4.7 are required to exceed 35, 30, 25, and 20 GeV for the first-, second-, third-, and fourth-leading jet, respectively. Differential cross sections are measured as functions of the jet transverse momentum, jet pseudorapidity, and several other observables that describe the angular correlations between the jets. The measured distributions show sensitivity to different aspects of the underlying event, parton shower modeling, and matrix element calculations. In particular, the interplay between angular correlations caused by parton shower and double-parton scattering contributions is shown to be important. The double-parton scattering contribution is extracted by means of a template fit to the data, using distributions for single--parton scattering obtained from Monte Carlo event generators and a double-parton scattering distribution constructed from inclusive single-jet events in data. The effective double-parton scattering cross section is calculated and discussed in view of previous measurements and of its dependence on the models used to describe the single-parton scattering background.

JOURNAL OF HIGH ENERGY PHYSICS [1], 177, 2022. DOI: 10.1007/JHEP01(2022)177

[P018-2022] "Measurement of inclusive charged-particle b--jet production in pp and p-Pb collisions at root S-NN =5.02 TeV"

Acharya, S.; Adamova, D.; **Chinellato, D. D.*; Guardiano, G. G.*; Jahnke, C.*; Takahashi, J.***; et al. ALICE Collaboration

A measurement of the inclusive b-jet production cross section is presented in pp and p-Pb collisions at root S-NN = 5.02 TeV, using data collected with the ALICE detector at the LHC. The jets were reconstructed in the central rapidity region vertical bar eta vertical bar < 0.5 from charged particles using the anti-kT algorithm with resolution parameter R = 0.4. Identification of b jets exploits the long lifetime of b hadrons, using the properties of secondary vertices and impact parameter distributions. The p(T)-differential inclusive production cross section of b jets, as well as the corresponding inclusive b-jet fraction, are reported for pp and p-Pb collisions in the jet transverse momentum range 10 <= p(T)(,)(ch) (jet) <= 100 GeV/c, together with the nuclear modification factor, R-pPb(b-jet). The analysis thus extends the lower p(T) limit of b-jet measurements at the LHC. The nuclear modification factor is found to be consistent with unity, indicating that the production of b jets in p-Pb at root S-NN = 5.02 TeV is not affected by cold nuclear matter effects within the current precision. The measurements are well reproduced by POWHEG NLO pQCD calculations with PYTHIA fragmentation.

JOURNAL OF HIGH ENERGY PHYSICS [1], 178, 2022. DOI: 10.1007/JHEP01(2022)178

[P019-2022] "Measurement of Prompt D 0, Λ+c, and Σ 0, ++c (2455) Production in Proton-Proton Collisions at √ s=13 TeV"

Acharya, S.; Adamova, D.; **Chinellato, D. D.*; Guardiano, G. G.*; Jahnke, C.*; Takahashi, J.***; et al. ALICE Collaboration

The p(T)-differential production cross sections of prompt D-0, Lambda(c)+, and Sigma(0,++)(c) (2455) charmed hadrons are measured at midrapidity (vertical bar y vertical bar < 0.5) in pp collisions at root s. = 13 TeV. This is the first measurement of Sigma(0,++)(c) production in hadronic collisions. Assuming the same production yield for the three Sigma(0,++)(c) isospin states, the baryon-to-meson cross section ratios Sigma(0,+,++)(c)/D-0 and Lambda(+)(c)/D-0 are calculated in the transverse momentum (p(T)) intervals 2 < p(T) < 12 and 1 < p(T) < 24 GeV/c. Values significantly larger than in e(+) e(-) collisions are observed, indicating for the first time that baryon enhancement in hadronic collisions also extends to the Sigma(c). The feed-down contribution to Lambda(+)(c) production from Sigma(0,+,++)(c) is also reported and is found to be larger than in e(+)e(-) collisions. The data are compared with predictions from event generators and other phenomenological models, providing a sensitive test of the different charm-hadronization mechanisms implemented in the models.

PHYSICAL REVIEW LETTERS 128[1], 012001, 2022. DOI: 10.1103/PhysRevLett.128.012001

[P020-2022] "Mechanical response of pentadiamond: A DFT and molecular dynamics study"

Felix, L. C.*; Tromer, R. M.*; Woellner, C. F.; Tiwary, C. S.; **Galvao, D. S.***

Pentadiamond is a recently proposed new carbon allotrope consisting of a network of pentagonal rings where both sp2 and sp3 hybridization are present. In this work we investigated the mechanical and electronic properties, as well as, the thermal stability of pentadiamond using DFT and fully atomistic reactive molecular dynamics (MD) simulations. We also investigated its properties beyond the elastic regime for three different deformation modes: compression, tensile and shear. The behavior of pentadiamond under compressive deformation showed strong fluctuations in the atomic positions which are responsible for the strain softening at strains beyond the linear regime, which characterizes the plastic flow. As we increase temperature, as expected, Young's modulus values decrease, but this variation (up to 300 K) is smaller than 10% (from 347.5 to 313.6 GPa), but the fracture strain is very sensitive, varying from -44% at 1 K to -5% at 300 K.

PHYSICA B-CONDENSED MATTER 629, 413576, 2022. DOI: 10.1016/j.physb.2021.413576

[P021-2022] "Membrane model as key tool in the study of glutathione-s-transferase mediated anticancer drug resistance"

Materon, E. M.; **Shimizu, F. M.***; Santos, K. F. dos; Nascimento, G. F.; Geraldo, V. P. N.; Oliveira Junior, O. N.; Faria, R. C.

Glutathione-s-transferase is believed to be involved in the resistance to chemotherapeutic drugs, which depends on the interaction with the cell membranes. In this study, we employed Langmuir monolayers of a mixture of phospholipids and cholesterol (MIX) as models for tumor cell membranes and investigated their interaction with the anticancer drugs cisplatin (CDDP) and doxorubicin (DOX). We found that both DOX and CDDP expand and affect the elasticity of MIX monolayers, but these effects are hindered when glutathione-s-transferase (GST) and its cofactor glutathione (GSH) are incorporated. Changes are induced by DOX or CDDP on the polarizationmodulated infrared reflection absorption spectroscopy (PM-IRRAS) data for MIX/GST/GSH monolayers, thus denoting some degree of interaction that is not sufficient to alter the monolayer mechanical properties. Overall, the results presented here give support to the hypothesis of the inactivation of DOX and CDDP by GST and point to possible directions to detect and fight drug resistance.

BIOMEDICINE & PHARMACOTHERAPY 145, 112426, 2022. DOI: 10.1016/j.biopha.2021.112426

[P022-2022] "Metamagnetic transitions induced by doping with non-magnetic 4+ions in ludwigites Co(5)A(O2BO3)(2) (A=Zr and Hf)"

Mariano, D. L.; Heringer, M. A. V.; Freitas, D. C.; **Andrade, V. M.***; Saitovitch, E. B.; Continentino, M. A.; Ghivelder, L.; Passamani, E. C.; Sanchez, D. R.

The novel A-doped Co3O2BO3 (A(4+)=Zr, Hf) ludwigites have been synthetized by the first time and investigated by X-ray diffraction, magnetization and specific heat experiments. The non-magnetic ions place mainly at sites 4 of the structure. This doping strengthens the magnetic interactions rising the magnetic transition temperatures from 42 K, for the undoped compound, to 71 K and 72 K for Zr and Hf, respectively. These magnetic transition temperature are 10 K below that shown by the Sn4+-doped Co3O2BO3. As expected, all these isostructural and isovalent compounds exhibit the same magnetic features. However, low temperature specific heat experiments and magnetization curves with typical metamagnetic behavior revealed that doping with the non-magnetic open-shell ions d(0) Zr and Hf preserves the two-dimensional antiferromagnetic character of the parent ludwigite Co3O2BO3 while the closed-shell d(10)Sn leads to a three-dimensional magnetism. The experimental results are compatible with an antiferromagnetic structure with a ferromagnetic component for these two compounds. The difference in T-N and dimensionality of these compounds are related to super-superexchange (SSE) interaction between two Co2+ mediated by the nonmagnetic ion A(4+). The non--magnetic closed-shell d(10) ion turned out to be more effective in mediating SSE interactions between 1-2-3 magnetic layers.

JOURNAL OF ALLOYS AND COMPOUNDS 890, 161717, 2022. DOI: 10.1016/j.jallcom.2021.161717

[P023-2022] "Microscopic probe of magnetic polarons in antiferromagnetic Eu5In2Sb6"

Souza, J. C.*; Thomas, S. M.; Bauer, E. D.; Thompson, J. D.; Ronning, F.; **Pagliuso, P. G.***; Rosa, P. F. S.

Colossal magnetoresistance (CMR) emerges from intertwined spin and charge degrees of freedom in the form of ferromagnetic clusters also known as trapped magnetic polarons. As a result, CMR is rarely observed in antiferromagnetic materials. Here we use electron spin resonance (ESR) to reveal microscopic evidence of the formation of magnetic polarons in antiferromagnetic Eu5In2Sb6. First, we observe a reduction of the Eu2+ ESR linewidth as a function of the applied magnetic field consistent with ferromagnetic clusters that are antiferromagnetically coupled. Additionally, the Eu2+ line shape changes markedly below T' similar to 200 K, a temperature scale that coincides with the onset of CMR. The combination of these two effects provides strong evidence that magnetic polarons grow in size below T' and start influencing the macroscopic properties of the system.

PHYSICAL REVIEW B 105[3], 035135, 2022. DOI: 10.1103/PhysRevB.105.035135

[P024-2022] "Eavesdropping on the Decohering Environment: Quantum Darwinism, Amplification, and the Origin of Objective Classical Reality"

Touil, A.; Yan, B.; Girolami, D.; **Deffner, S.*;** Zurek, W. H.

"How much information about a system S can one extract from a fragment F of the environment E that decohered it?" is the central question of Quantum Darwinism. To date, most answers relied on the quantum mutual information of SF, or on the Holevo bound on the channel capacity of F to communicate the classical information encoded in S. These are reasonable upper bounds on what is really needed but much harder to calculate-the accessible information in the fragment F about S. We consider a model based on imperfect C-NOT gates where all the above can be computed, and discuss its implications for the emergence of objective classical reality. We find that all relevant quantities, such as the quantum mutual information as well as various bounds on the accessible information exhibit similar behavior. In the regime relevant for the emergence of objective classical reality this includes scaling independent of the quality of the imperfect C-NOT gates or the size of E, and even nearly independent of the initial state of S.

PHYSICAL REVIEW LETTERS 128[1], 010401, 2022. DOI: 10.1103/PhysRevLett.128.010401

[P025-2022] "Orbital localization and the role of the Fe and As 4p orbitals in BaFe2As2 probed by XANES"

Figueiredo, A. G. de; Cantarino, M. R.; Silva Neto, W. R. da; **Pakuszewski, K. R.*; Grossi, R.*; Christovam, D. S.*; Souza, J. C.*; Piva, M. M.*; Freitas, G. S.*; Pagliuso, P. G.*; Adriano, C.*; Garcia, F. A.***

The polarization dependence of the near edge x-ray absorption spectroscopy (XANES) is an element specific probe to the real-space distribution of the density of unoccupied states in solid-state materials. In this paper, we present Fe and As K--edge experiments of Ba(Fe1-xMx)2As2 (M = Mn, Co, and x = 0.0 and 0.08). The experiments reveal a strong polarization dependence of the probed XANES spectra, which concerns mainly an increase in the intensity of electronic transitions when the beam polarization is set out of the sample's ab crystallographic plane. The results show that states with pz--orbital character dominate the density of unoccupied states close to the Fermi level. Partial substitution of Fe by Co is shown to decrease the intensity anisotropy, suggesting that Co promotes electronic transfer preferentially to states with pz--orbital character. On the other hand, Mn substitution causes the increase in the spectra pz-orbital anisotropy, which is proposed to take place by means of an enhanced local Fe 3d4p mixing, unveiling the role of Fe 4p states in the localization of the Fe 3d orbitals. Moreover, by comparing our results to previous experiments, we identify the relative mixing between Fe and pnictide 4px,y,z orbitals as a clear divide between the electronic properties of iron arsenides and selenides. Our conclusions are supported by multiple-scattering theory calculations of the XANES spectra and by quantum chemistry calculations of the Fe coordination electronic structure.

PHYSICAL REVIEW B 105[4], 045130, 2022. DOI: 10.1103/PhysRevB.105.045130

[P026-2022] "Production of light (anti)nuclei in pp collisions at root s=13 TeV"

Acharya, S.; Adamova, D.; **Chinellato, D. D.*; Guardiano, G. G.*; Jahnke, C.*; Takahashi, J.***; et al. ALICE Collaboration

Understanding the production mechanism of light (anti)nuclei is one of the key challenges of nuclear physics and has important consequences for astrophysics, since it provides an input for indirect dark-matter searches in space. In this paper, the latest results about the production of light (anti) nuclei in pp collisions at root s = 13TeV are presented, focusing on the comparison with the predictions of coalescence and thermal models. For the first time, the coalescence parameters B-2 for deuterons and B-3 for helions are compared with parameter-free theoretical predictions that are directly constrained by the femtoscopic measurement of the source radius in the same event class. A fair description of the data with a Gaussian wave function is observed for both deuteron and helion, supporting the coalescence mechanism for the production of light (anti)nuclei in pp collisions. This method paves the way for future investigations of the internal structure of more complex nuclear clusters, including the hypertriton.

JOURNAL OF HIGH ENERGY PHYSICS [1], 106, 2022. DOI: 10.1007/JHEP01(2022)106

[P027-2022] "Revisiting Quasicrystals for the Synthesis of 2D Metals"

Yadav, T. P.; Kumbhakar, P.; Mukhopadhyay, N. K.; **Galvao, D. S.***; Ajayan, P. M.; Ranganathan, S.; Chattopadhyay, K.; SekharTiwary, C.

Quasicrystals (QCs) are intermetallic materials with long-range ordering but with lack of periodicity. They have attracted much interest due to their interesting structural complexity, unusual physical properties, and varied potential applications. The last four decades of research have demonstrated the existence of different forms of QC composed of several metallic and non-metallic systems, which have already been exploited in several applications. Recently, with the experimental realization of 2D (atomically thin) metals, the potential applications of these structures have significantly increased (such as inflexible electronics, optoelectronics, electrocatalysis, strain sensors, nano-generators, innovative nano-electromechanical systems, and biomedical applications). As a result, high-quality 2D metals and alloys with engineered and tunable properties are in great demand. This review summarizes the recent advances in the synthesis of 2D single and few layered metals and alloys using quasicrystals. These structures present a large number of active sites for hydrogen evolution process catalysis and other functional properties. In this review, we also highlighted the possibility of using QC to synthesize other 2D metals and to explore their physical and chemical properties.

TRANSACTIONS OF THE INDIAN INSTITUTE OF METALS, Early Access: JAN 2022. DOI: 10.1007/s12666-021-02506-0

[P028-2022] "Series Expansion of the Excess Work Using Nonlinear Response Theory"

Naze, P.*; Bonanca, M. V. S.*

The calculation of observable averages in non-equilibrium regimes is one of the most important problems in statistical physics. Using the Hamiltonian approach of nonlinear response theory, we obtain a series expansion of the average excess work and illustrate it with specific examples of thermally isolated systems. We report the emergence of non-vanishing contributions for large switching times when the system is subjected to strong driving. The problem is solved by using an adapted multiple--scale method to supress these secular terms. Our paradigmatic examples show how the method is implemented generating a truncated series that obeys the Second Law of Thermodynamics.

JOURNAL OF STATISTICAL PHYSICS 186[2], 23, 2022. DOI: 10.1007/s10955-021-02869-0

[P029-2022] "Size and doping effects on the improvement of the low-temperature magnetic properties of magnetically aligned cobalt ferrite nanoparticles"

Tancredi, P.; Rivas-Rojas, P. C.; Moscoso-Londono, O.; **Muraca, D.*; Knobel, M.*;** Socolovsky, L. M.

The macroscopic magnetic behavior of nanoparticulated systems is the result of several contributions, ranging from the intrinsic structural properties of the nanoparticles to their spatial arrangement within the material. Unravelling and understanding these influences is an important task to produce nano-systems with improved properties for specific technological applications. In this work we study how the magnetic behavior of a set of magnetically hard nanoparticles can be improved by the modification of the sample arrangement (either randomly or magnetically oriented) and the nature of the enclosing matrices. At first, we employed a hot-injection, continuous growth strategy to synthesize non-stoichiometric cobalt ferrite (CoxFe(3-x) O(4)) nanoparticles. We prepared five batches of hydrophobic, oleate-coated samples, with mean diameters of 8 nm, 12 nm, 16 nm and variable Co-to-Fe proportions. The structural characterization con-firms that the nanoparticles have a spinel--type monocrystalline structure and that the Co and Fe ions are homogenously distributed within the system. The magnetic properties of the nanoparticles were measured by DC magnetometry, and we found that the strategy used in this work to create a system of magnetically oriented nanoparticles can lead to a significant remanence and coercive field enhancement at low temperatures when compared with randomly oriented and fixed systems. The modification of the magnetic properties was detected in the five batches of samples, but the strength of the enhancement depends on both size and composition of the nanoparticles. Indeed, for the "hardest" samples the coercive field of the magnetically oriented systems reached values of around 30 kOe (3 T), which represents a 50% increase regarding the randomly oriented system and are among the highest reported to date for a set of Fe and Co oxide nanoparticles.

JOURNAL OF ALLOYS AND COMPOUNDS 894, 162432, 2022. DOI: 10.1016/j.jallcom.2021.162432

[P030-2022] "Strong subadditivity lower bound and quantum channels"

Mendes, L. R. S.*; Oliveira, M. C. de*

We derive the strong subadditivity of the von Neumann entropy with a strict lower bound, dependent on the distribution of quantum correlation in the system. We investigate the structure of states saturating the bounded subadditivity and examine its consequences for the quantum data processing inequality. The quantum data processing achieves a lower bound associated with the locally inaccessible information.

QUANTUM INFORMATION PROCESSING 21[2], 78, 2022. DOI: 10.1007/s11128-022-03419-7

[P031-2022] "Surface structure characterization of a (root 5 x root 5)-R26.6 degrees reconstruction of strontium titanate (001) by X-ray photoelectron diffraction"

Pancotti, A.; Silva, J. J.; **Siervo, A. de*; Landers, R.***; Nascente, P. A. P.

The surface composition of a (root 5 x root 5)-R26.6 degrees (Rt5) reconstruction of a strontium titanate (001) single crystal surface was characterized by X-ray photoelectron spectroscopy (XPS), and its atomic surface structure was determined by a combination of low energy electron diffraction (LEED) and X-ray photoelectron diffraction (XPD). The comparison between experimental and theoretical XPD results involving multiple scattering calculations indicated that the analyzed Rt5 reconstruction of the SrTiO3 (001) surface has two possible terminations: 40% of SrO and 60% of TiO2.

SURFACE SCIENCE 715, 121937, 2022. DOI: 10.1016/j.susc.2021.121937

[P032-2022] "The DES view of the Eridanus supervoid and the CMB cold spot"

Kovacs, A.; Jeffrey, N.; **Navarro-Alsina, A.***; et al.

The Cold Spot is a puzzling large-scale feature in the Cosmic Microwave Background temperature maps and its origin has been subject to active debate. As an important foreground structure at low redshift, the Eridanus supervoid was recently detected, but it was subsequently determined that, assuming the standard Lambda CDM model, only about 10-20 per cent of the observed temperature depression can be accounted for via its Integrated Sachs-Wolfe imprint. However, R greater than or similar to 100 h(-1)Mpc supervoids elsewhere in the sky have shown ISW imprints A(ISW) approximate to 5.2 +/- 1.6 times stronger than expected from Lambda CDM (A(ISW) = 1), which warrants further inspection. Using the Year-3 redMaGiC catalogue of luminous red galaxies from the Dark Energy Survey, here we confirm the detection of the Eridanus supervoid as a significant underdensity in the Cold Spot's direction at z < 0.2. We also show, with S/N greater than or similar to 5 significance, that the Eridanus supervoid appears as the most prominent large-scale underdensity in the dark matter mass maps that we reconstructed from DES Year-3 gravitational lensing data. While we report no significant anomalies, an interesting aspect is that the amplitude of the lensing signal from the Eridanus supervoid at the Cold Spot centre is about 30 per cent lower than expected from similar peaks found in N-body simulations based on the standard Lambda CDM model with parameters Omega(m) = 0.279 and sigma(8) = 0.82. Overall, our results confirm the causal relation between these individually rare structures in the cosmic web and in the CMB, motivating more detailed future surveys in the Cold Spot region.

MONTHLY NOTICES OF THE ROYAL ASTRONOMICAL SOCIETY 510[1], 216-229, 2022. DOI: 10.1093/mnras/stab3309

[P033-2021] "Tunable Anomalous Scattering and Negative Asymmetry Parameter in a Gain-Functionalized Low Refractive Index Sphere"

Ali, R.*

Usually, low refractive index passive spheres exhibit strong forward scattering and a positive asymmetry parameter due to weak interference between the electric and magnetic scattering channels. In this work, we investigate, analytically and numerically, the forward scattering of light by a gain--functionalized low refractive index dielectric sphere. It is shown that by tuning the optical gain one can optimize the interference, which provides a novel paradigm to achieve the zero forward scattering and negative asymmetry parameter even for a low refractive index sphere. As a result, a low-density collection of such identical back scatterers provides an anomalous regime, where the scattering mean free path and extinction mean free path are greater than the transport mean free path. Furthermore, we also provide the numerical guideline to achieve the larger extinction mean free path without achieving preferential back-scattering.

ACS OMEGA, Early Access: JAN 2022. DOI: 10.1021/acsomega.1c05662

Aceitos para publicação

[A001-2022] "Effective acetylene length dependence of the elastic properties of different kinds of graphynes"

Kanegae, G. B.*; Fonseca, A. F.*

Graphyne is a planar network of connected carbon chains, each formed by n acetylene linkages. Uncountable ways to make these connections lead to uncountable structural graphyne families (GFs). As the synthesis of graphynes with n > 1 has been reported in literature, it is of interest to find out how their physical properties depend on n for each possible GF. Although literature already present specific models to describe the dependence on n of the elastic properties of specific GFs, there is not yet enough amount of data for the physical properties of different graphynes with different values of n. Based on fully atomistic molecular dynamics simulations, the Young's modulus, shear modulus, linear compressibility and Poisson's ratio of 10 graphyne members of 7 different GFs are calculated. A simple elastic model consisting of a serial combination of n springs is proposed to describe the dependence on n of the elastic properties of these 7 GFs. We show that except for the Poisson's ratio, this simple unique elastic model is able to numerically describe, with good precision, the Young's modulus, shear modulus and linear compressibility of all different graphynes, including anisotropy and negative values of linear compressibility of some GFs.

CARBON TRENDS 7, 100152, April 2022. DOI: 10.1016/j.cartre.2022.100152

***Autores da comunidade IFGW**
Fonte: Web of Science on-line (WOS)

Observação: Não ocorreram neste período defesas de teses e dissertações, com orientadores ou banca do IFGW, do Programa de Pós-Graduação Multiunidades em Ensino de Ciências e Matemática – Mestrado e Doutorado (PECIM) da Unicamp.

Fonte: Página do PECIM
Disponível em: https://www.pecim.unicamp.br/bancas

Defesas de Dissertações do IFGW

[D001-2022] "Absorção Multifóton em Heteroestruturas baseadas em CdSe"
Aluno: Arthur Aló de Oliveira
Orientador: Prof. Dr. Lázaro Aurélio Padilha Júnior
Data: 12/01/2022

[D002-2022] "Efeitos da Localização do Núcleo nas Propriedades Foto-Física de Nanoestruturas tipo Ponto-em-Bastão de CdSe/CdS"
Aluno: Jonathan Cotrino Lemus
Orientador: Prof. Dr. Lázaro Aurélio Padilha Júnior
Data: 27/01/2022

Defesas de Teses do IFGW

[T001-2022] "Darwinismo Quântico e Contextualidade"
Aluno: Roberto Dobal Baldijão
Orientador: Prof. Dr. Marcelo de Oliveira Terra Cunha
Data: 03/02/2022

[T002-2022] "Estudo de desenvolvimento de biossensor óptico de alta sensibilidade e baixa dependência a variações de temperatura"
Aluno: André Luis Morás Júnior
Orientador: Prof. Dr. Newton Frateschi
Data: 03/02/2022

[T003-2022] "Caracterização das alterações hemodinâmicas medidas por NIRS em doenças com comprometimento vascular"
Aluno: Andres Fabian Quiroga Soto
Orientador: Prof. Dr. Rickson Mesquita
Data: 04/02/2022

Fonte: Portal IFGW/Pós-graduação - Agenda de Colóquios, Defesas e Seminários.
Disponível em: http://portal.ifi.unicamp.br/pos-graduacao

Abstracta

Instituto de Física
Diretor: Profa. Dra. Mônica Alonso Cotta
Diretora Associada: Prof. Dr. Marcos Cesar de Oliveira
Universidade Estadual de Campinas - UNICAMP
Cidade Universitária Zeferino Vaz
13083-859 - Campinas - SP - Brasil
e-mail: secdir@ifi.unicamp.br
Fone: +55 19 3521-5300

Publicação

Biblioteca do Instituto de Física Gleb Wataghin
http://portal.ifi.unicamp.br/biblioteca
Instagram: @bif.unicamp
Telegram: t.m/bifunicamp

Diretora Técnica: Sandra Maria Carlos Cartaxo
Coordenadora da Comissão de Biblioteca: Profa. Dra. Arlene Cristina Aguilar

Elaboração:
Maria Graciele Trevisan (Bibliotecária)
contato: infobif@ifi.unicamp.br